A widespread family of ribosomal peptide metallophores involved in bacterial adaptation to copper stress

Laura Leprevost*[1], Sophie Jünger*[2], Guy Lippens[3], Céline Guillaume[2], Giuseppe Sicoli[4], Lydie Oliveira[5], Alex Rivera-Millot[1&], Gabriel Billon[4], Céline Henry[5], Rudy Antoine[#1], Svetlana Dubiley[#3], Séverine Zirah[#2], Yanyan Li[#2], Françoise Jacob-Dubuisson[#1]

[1] Univ. Lille, U1018-UMR9017-CIIL-Center for infection and Immunity of Lille, F-59000 Lille, FRANCE

[2] Unit Molecules of Communication and Adaptation of Microorganisms (MCAM), UMR 7245 CNRS, MNHN, Alliance Sorbonne University, 75005 Paris, FRANCE

[3] Toulouse Biotechnology Institute, CNRS/INRAE/INSA/UPS, 31077 Toulouse, FRANCE

[4] Univ. Lille, CNRS, UMR 8516 - LASIRE, Laboratoire de Spectroscopie pour les Interactions, la Réactivité et l'Environnement F-59000 Lille, FRANCE

[5] INRAE-AgroParisTech-Univ. Paris-Saclay, MICALIS, 78352 Jouy-en Josas, FRANCE

[*] contributed equally

[#] for correspondence: rudy.antoine@pasteur-lille.fr; svetlana.dubiley@gmail.com; severine.zirah@mnhn.fr; yanyanli@mnhn.fr; francoise.jacob@ibl.cnrs.fr

[&] current address: INRS-Centre Armand-Frappier Santé Biotechnologie, Bacterial Symbionts Evolution, Laval, Quebec H7V 1B7, Canada

Abstract

Ribosomally synthesized, post-translationally modified peptides (RiPPs) are increasingly known to play prominent roles in bacterial adaptation. Herein, we identified and characterized a family of RiPP metallophores with rare 5-thiooxazole motifs, whose production is induced by transition metal stress in a number of pathogenic and environmental bacteria. Using *Caulobacter vibrioides* as a model, we demonstrated that the so-called bufferins confer protection to the bacteria from copper by complexing with the metal. Bufferin biosynthesis requires a multinuclear non-heme iron-dependent oxidase (MNIO, DUF692 family) and its partner protein to install thiooxazoles on Cys residues. By contrast, a hallmark feature of bufferin precursors, the N-terminal signal peptide sequence, is not essential for this transformation. Bufferin-like gene clusters are widespread in Eubacteria, including several pathogens, and the *C. vibrioides* epitomize the largest two families of RiPPs involving MNIO enzymes. Our study unveils a widespread but overlooked bacterial strategy mediated by a new type of RiPPs to cope with copper stress encountered in the environment and in the phagosomes of predatory protists or mammalian hosts.

Introduction

Microorganisms are endowed with an immense capacity of adaptation to their environments, both biotic and abiotic. One strategy is the production of specialised metabolites which play key roles in microbial adaptive processes, including defence against competing species, nutrient acquisition and resistance to stresses (1). Bacterial metallophores are prominent examples that can promote bacterial growth under different conditions (2-5). Several transition metals, including copper, are essential for living organisms (6, 7). However, the excess of copper is toxic to cells, because its high affinity for organic molecules results in the inactivation of essential pathways (7-9). Bacteria encounter copper in natural habitats and within phagocytic

55 cells, which use it as a microbicidal agent (10, 11). Therefore, they have developed an arsenal
56 of defence systems, including tight regulation of copper uptake, various export systems, and
57 sequestration/storage by copper-chelating molecules or proteins (12, 13). For pathogens, these
58 strategies are critical for host infection by enhancing their survival in phagocytes, and hence
59 they are linked to virulence (14).

60 Previous work on the whooping cough agent *Bordetella pertussis* has identified a four-gene
61 operon (BP2924-BP2927) controlled by BvgAS, the master two-component system that
62 regulates most virulence factors (15). This biosynthetic gene cluster (BGC) is similar to the *gig*
63 (gold-induced genes) operons of *Cupriavidus metallidurans* and *Legionella pneumophila* and
64 to a related operon of *Caulobacter vibrioides* (formerly *Caulobacter crescentus*) (16-18)
65 (Extended Fig. 1A). These operons except for that of *B. pertussis* are up-regulated upon
66 exposure to transition metals, notably copper (16-19). Although these data suggest a role for
67 *gig*-like genes in copper stress response, the function and the nature of derived biomolecules
68 have remained a mystery.

69 Ribosomally synthesized and post-translationally modified peptides (RiPPs) are natural
70 products with a tremendous variety of structures and biological activities (1, 20, 21). They are
71 synthesized from a gene-encoded precursor peptide, generally composed of an N-terminal
72 leader sequence and a core sequence where post-translational modifications (PTMs) occur. In
73 many cases, a RiPP recognition element (RRE) domain encoded in the same BGC interacts
74 with the leader sequence and serves as a docking site for the modification enzymes (22, 23).
75 RRE domains are thus a hallmark feature of RiPP biosynthesis. The vast structural diversity of
76 RiPPs is conferred by unlimited possibilities of chemical transformations. An emerging family
77 of PTM enzymes is the DUF692 family of multinuclear non-heme iron dependent oxidases
78 (MNIOs) that catalyse various reactions mostly but not exclusively on Cys residues, in the

79 biosynthesis of specific RiPPs (24-30). However, the full spectrum of reactions catalysed by
80 MNIO enzymes remains far from being fully appreciated.
81 Here we report the first functional and structural characterization of the molecules produced
82 by *gig*-like operons using *C. vibrioides* as a model. They represent a new family of RiPP
83 metallophores with 5-thiooxazole modifications installed by MNIOs and contribute to bacterial
84 adaptation to excess copper by complexing with this metal. We suggest to name these peptides
85 bufferins.
86

87 ## Results

88 ***Gig-like operons belong to putative RiPP BGCs.*** To gain insight into gene function, *in silico*
89 analyses were performed on the CCNA_3363-3366 operon of *C. vibrioides*, hereafter named
90 *buf1*. CCNA_3363 encodes a DUF2282-family protein (BufA1), whose members are 80-120
91 residues long and harbour four Cys residues and a predicted N-terminal, Sec-dependent signal
92 peptide (Fig. 1A; Extended Fig. 1A,B). The product of CCNA_3364 (BufB1) belongs to the
93 MNIO superfamily, whereas CCNA_3365 codes for a protein (BufC1) with an N-terminal
94 DUF2063 domain of unknown function. Importantly, the C-terminal domain of BufC1 is
95 predicted to be structurally related to RRE domains (Extended Fig. 1C). Finally, CCNA_3366
96 encodes a DoxX-type oxido-reductase (BufD1) (31, 32). The other *gig*-like operons share the
97 same gene organizations and predicted functions. In light of the recent discovery of MNIOs
98 involved in RiPP biosynthesis (24-30), we hypothesized that BufB1 and BufC1 would install
99 modifications on Cys residues of BufA1. Upstream of *bufA1*, CCNA_3362 and CCNA_3361
100 encoding the extracytoplasmic function (ECF)-family sigma factor SigF and the anti-sigma
101 protein NrsF were also found to be induced by copper stress (19) and are therefore part of the
102 *buf1* BGC. Inspection of the *C. vibrioides* genome identified a second *buf2* BGC (CCNA_2999-
103 3001) which is also part of the SigF regulon (Fig. 1A). It encodes homologues of BufB1

104 (CCNA_3000) and BufC1 (CCNA_2999) but lacks a *doxX* gene. Its precursor peptide BufA2
105 (CCNA_3001) possesses a signal peptide, like BufA1, but its core sequence displays 6 Cys
106 residues and is without family signature (Extended Fig. 1C).
107
108 ***Bufferins are involved in adaptation to excess copper***. In *C. vibrioides*, the *buf1* and *buf2*
109 BGCs belong to the SigF-controlled, core regulon of copper stress (17, 19, 33). The former was
110 also reported to respond to chromate and cadmium ions. These data suggest a link of the *buf*
111 operons with metal response. To test if they could be up-regulated by other transition metals,
112 we generated reporter fusions within *bufA1* and *bufA2* and confirmed that both are induced by
113 Cu^{2+} but not Fe^{2+}, Zn^{2+} or Mn^{2+} (Suppl. Fig. S1). As copper indirectly generates oxidative stress,
114 we also tested oxidants and identified HOCl as a weak inducer.
115 To determine if bufferins, the putative RiPP products of the *buf* BGCs, contribute to
116 adaptation to copper stress, we generated *C. vibrioides* deletion mutants that express one (Cv_{buf1}
117 and Cv_{buf2}) or neither BGC (Cv_{DKO}). Cv_{DKO} grew more slowly than the parental Cv_{WT} wild-
118 type strain when $CuSO_4$ was added to the growth medium, unlike Cv_{buf1} or Cv_{buf2} (Fig. 1B).
119 This indicates that bufferins enhance growth under copper stress and that they are functionally
120 redundant. To confirm that a single BCG is sufficient to protect bacteria from excess copper,
121 we performed a gain-of-function experiment in an *Escherichia coli* laboratory strain. For this,
122 we expressed the *buf1ABCD* operon under the control of a PT5-lac promoter upon IPTG
123 induction. Expression of *buf1ABCD* enhanced survival of *E. coli* exposed to a bactericidal
124 concentration of $CuSO_4$ (Fig. 1C).
125 We then asked whether the protection from copper would confer an advantage on *C.*
126 *vibrioides* in biotic interactions. As amoeba notably use copper against their bacterial preys, a
127 predation assay was performed (10). Attempts to measure survival of *C. vibrioides* after
128 ingestion by *Dictyostelium discoidum* were unsuccessful. Therefore, we tested if the presence

129 of the *buf* BGCs might slow down bacterial killing. We placed amoebal suspensions onto
130 bacterial lawns, and after incubation we determined bacterial densities in the contact zones by
131 densitometry scanning. Larger zones of complete bacterial lysis were observed for the Cv_{DKO}
132 than for the Cv_{WT} strain, consistent with a protective role of bufferins (Fig. 1D).
133
134 ***Features of buf BGCs required for function***. To pinpoint key *buf* genes in the function of
135 bufferins, we constructed Cv_{buf1} derivatives that lack one or several genes ($Cv_{buf1(A)}$, $Cv_{buf1(ACD)}$,
136 $Cv_{buf1(ABD)}$, $Cv_{buf1(ABC)}$ and $Cv_{buf1(BCD)}$) and tested their growth phenotypes. Growth of all
137 deletion strains except for $Cv_{buf1(ABC)}$ was sluggish in the presence of $CuSO_4$, showing that
138 BufA1, BufB1 and BufC1 but not BufD1 are required for function in these growth conditions
139 (Fig. 2A). Similarly, the deletion of *bufB2* and *bufC2* in Cv_{buf2} impacted bacterial growth in the
140 presence of $CuSO_4$ (Fig. 2A).
141 As BufA1 harbours four conserved Cys residues (Cys^{I} to Cys^{IV}) that might be targets of
142 PTMs, we replaced them with Ser, separately or in combination and introduced the mutant
143 genes in the Cv_{buf1} chromosome by allelic exchange. All resulting strains $Cv_{buf1}^{CysISer+CysIVSer}$,
144 $Cv_{buf1}^{CysIISer+CysIIISer}$, $Cv_{buf1}^{CysIISer}$ and $Cv_{buf1}^{CysIIISer}$ grew more slowly in the presence of $CuSO_4$
145 than Cv_{buf1} (Fig. 2B), indicating the importance of the four Cys residues for function.
146
147 ***Characterization of PTMs on bufferins***. To identify the PTMs on bufferins, we engineered an
148 IPTG-inducible version of SigF to control expression of their BGCs in *C. vibrioides*. The
149 metabolic profiles of IPTG-treated Cv_{buf1}(pSigF) and Cv_{buf2}(pSigF) were analysed by liquid
150 chromatography coupled to mass spectrometry (LC-MS) and compared to that of Cv_{DKO}(pSigF)
151 to reveal peptide species only present in the *buf*-expressing strains. In Cv_{buf1}(pSigF), a major
152 species exhibited masses corresponding to BufA1 with the signal peptide cleaved off and a
153 mass shift of -10 Da (Fig. 3A; Suppl. Fig. S2; Suppl. Table S1). Interestingly, a second form

154 with a mass shift of -12 Da was also detected, but not systematically, and it disappeared upon
155 storage or freeze-thawing. The most stable product with a -10 Da mass shift is considered the
156 mature peptide product and named Bufferin 1 (Buf1). Similarly, Cv_{buf2}(pSigF) produced a
157 major peptide product with a mass shift of -18 Da, called bufferin 2 (Buf2), and another species
158 with a -20 Da mass shift (Extended Fig. 2).

159 Reduction and alkylation treatment yielded species carrying three or four alkylating groups
160 for Buf1 and four, five or six alkylating groups for Buf2 (Extended Fig. 3), suggesting that the
161 PTMs result in alkylation-sensitive groups. MS analyses of trypsin-digested, alkylated bufferins
162 revealed that in Buf1, Cys^{I} and Cys^{IV} had mass increments corresponding to alkylation,
163 indicative of unmodified residues (Extended Fig. 4). By contrast, in the central tryptic peptide
164 AGENDCKAGAGTSCAGTSK containing Cys^{II} and Cys^{III}, both Cys residues carried mass
165 increments corresponding to alkylation with additional -4.03 Da mass shifts (Fig. 3B), as
166 proposed by the untargeted PTM search solution SpecGlobX (34). Altogether, the data are
167 consistent with the presence of a disulfide (S-S) bond between Cys^{I} and Cys^{IV} (resulting in -2
168 Da) and the central Cys^{II} and Cys^{III} being targets of 4-electron oxidation reactions (-4 Da each)
169 that generate alkylation-sensitive groups. Consistently, substitution of Cys^{II} or Cys^{III} with Ser
170 in Buf1 yielded peptides with mass shifts of -6 Da (Extended Fig. 5). Similarly, in Buf2, the
171 central Cys residues carry -4.03 Da shifts, while Cys^{I} and Cys^{IV} would form a disulfide bond
172 (Suppl. Fig. S3). Based on these data, we interpret the -12 Da and -20 Da species of Buf1 and
173 Buf2 (which will be named $Buf1^{ox}$ and $Buf2^{ox}$), respectively, as forms harbouring labile S-S
174 bonds between two alkylation-sensitive groups, in equilibrium with the bufferins.

175 To facilitate bufferin purification and characterization we added C-terminal strep or twin-
176 strep tags to BufA1. The affinity-purified proteins showed -10 Da mass shifts relative to the
177 calculated masses (Suppl. Fig. S4). To probe if the modified Cys residues may be part of
178 heterocycles as with other MNIO enzyme-catalysed PTMs (24, 27), we recorded UV-visible

179 absorption spectra of purified Buf1 and the Buf1$^{CysIISer+CysIIISer}$ variant. The spectrum of the
180 former showed a broad absorbance band extending to 310 nm, unlike that of the latter (Fig. 3C).
181 Similarly, the spectrum of recombinant Buf2 showed an absorbance maximum at 305 nm.
182 (Suppl. Fig. S5). These results are consistent with the presence of aromatic heterocycles (35).
183

184 ***Identification of the PTMs of Bufferin 1 by NMR***. To increase the yield of bufferin for
185 structural elucidation by NMR, we co-expressed *bufA1* carrying an N-terminal His_6-SUMO tag
186 with *bufB1* and *bufC1* in *E. coli* (Extended Fig. 6). Subsequent purification of modified BufA1
187 followed by trypsin digestion and preparative HPLC allowed to obtain the central 19-mer
188 peptide encompassing Cys^{II} (Cys23) and Cys^{III} (Cys31) at a milligram scale. Its ^{1}H spectrum
189 indicated two groups of anomalous resonances (Fig. 3D). By combining homonuclear ROESY
190 and TOCSY experiments (36) they were assigned to the NH protons of Lys24 and Ala32 that
191 follow the modified Cys23 and Cys31 residues, respectively, and to the Hα protons of Asp22
192 and Ser30 that precede these modified Cys residues (Extended Fig. 7A). The absence of both
193 Hα and NH protons for both Cys residues was verified on an ^{1}H, ^{15}N HSQC spectrum (Extended
194 Fig. 7B), indicating that their N and Cα atoms are part of heterocycles.

195 An ^{1}H, ^{13}C HMBC experiment showed correlations from the Asp22 and Ser30 Hα atoms
196 to carbon atoms at 161.1 ppm and 159.8 ppm, respectively (Extended Fig. 7C). Further
197 assignments were obtained with the uniformly ^{13}C,^{15}N-labeled 19-mer peptide and triple-
198 resonance NMR experiments (37, 38). In an HNCACB experiment we found no resonances
199 that could correspond to Lys24's upstream neighbour, confirming that the Cα of modified Cys^{II}
200 does not resonate at a typical 50-ppm value (Extended Fig. 8A). With an HNCO experiment,
201 we found values around 184 ppm for the C=O carbon atoms of both Cys residues (Extended
202 Fig. 8B), far from 175-ppm and 200-ppm values expected for such atoms in random-coil or
203 thio-amide peptides, respectively (39, 40). By increasing the resolution and varying the offset

204 of the decoupling pulse during the C=O evolution period, we determined a 90-Hz coupling
205 constant of these atoms with carbon atoms whose chemical shift is ~120 ppm, consistent with
206 their absence in the HNCACB experiment (Extended Fig. 8C). Both parameters point to the
207 C=O carbon atoms of the modified Cys connected to carbon atoms in aromatic rings (41).

208 The ^{13}C chemical shifts assigned on the modified peptide are in the same range as those for
209 the ring carbon atoms of a 5-thiooxazole-containing natural product (35). Together with the
210 anomalous chemical shift values for the Hα and NH protons of the flanking residues and taking
211 into account the MS data, we conclude that the modification leads to cyclization of both Cys to
212 form thiooxazole groups (Fig. 3E; Suppl. Text), consistent with their characteristic absorbance
213 maximum.

214

215 ***Copper binding by Bufferin 1.*** Given that heterocycles are prone to copper binding (5), we
216 interrogated if bufferins can complex with copper, which could be the basis for their protective
217 effect. To test this, purified $Buf1^{twstr}$ was incubated with $CuCl_2$ and analyzed by native MS. A
218 1:1 Buf1-Cu complex was detected (Suppl. Fig. S6), but the isotopic pattern suggested the
219 occurrence of both Buf1 and $Buf1^{ox}$, and the complexed/apo forms ratio varied between
220 experiments. We performed a spectroscopic binding assay with Buf1 to determine its affinity
221 constant for copper (42). However, formation of the complex appeared to be very slow,
222 suggesting an equilibrium between binding-competent and -incompetent bufferin forms (Suppl.
223 Fig. S6).

224 Therefore, we investigated complex formation *in vivo* by treating cultures of *bufA1*^{str}-
225 expressing *E. coli* with $CuSO_4$ for several hours prior to bufferin purification. Native MS
226 analysis showed that $Buf1^{str}$ thus produced was fully loaded with copper (Fig. 4A). This species
227 was further investigated by electron paramagnetic resonance (EPR). Pulsed EPR spectra

228 confirmed that bufferin 1 binds paramagnetic Cu^{2+}, and spectral simulations indicated
229 coordinating N atoms (43) (Fig. 4B; Suppl. Tables S2 and S3; Suppl. Fig. S7).

230 To gain insight into the copper binding site, we produced ^{15}N- and ^{15}N,^{13}C-labelled bufferin
231 samples and used 3-D spectra to assign the resonances. Simultaneously, we used the ^{1}H, ^{15}N
232 HSQC plane as a basis for HSQC-NOESY and TOCSY experiments to confirm the assignments
233 and gain some knowledge on structural aspects of bufferin. The sequential assignment was
234 interrupted by the modified Cys residues, as expected. Interestingly, amide resonances of the
235 tryptic peptide and of the same segment of the full-length bufferin do not correspond at all,
236 suggesting that the full-length sequence imposes structural constraints on the thiooxazole-
237 containing loop. Part of these likely come from the β sheet spanning two short strands in the
238 structural model, Thr9-Tyr13 and Trp44-Lys48 (Extended Fig. 9). The strong Hα(i-1) – HN(i)
239 NOE contacts between residues in these segments confirm their extended structure, and the
240 cross-strand NOE contacts between the amide protons of Lys45 and Cys12, and of Val47 and
241 Glu10, respectively, support their anti-parallel arrangement (Extended Fig. 9).

242 A comparison of the spectra of the bufferin produced with or without copper showed that
243 many peaks remained unchanged, others experienced a shift and some signal reduction, and yet
244 others disappeared altogether (Fig. 4C). The latter most probably concern residues close to the
245 paramagnetic Cu^{2+} ion. In particular, disappearance of the peaks corresponding to direct
246 neighbours of the thiooxazole heterocycles, Lys24, Ser30 and Ala32, strongly indicates that
247 these heterocycles are involved in Cu^{2+} coordination. Interestingly, signals of residues of the β-
248 sheet face oriented towards the thiooxazole-containing loop, Thr9, Trp44, Met46 and Lys48,
249 also disappeared in the spectrum of the complex. Whereas a full structural determination of
250 bufferin will require further experiments, our data support that the thiooxazole cycles and
251 residues of the β sheet are involved in copper binding.

252

253 ***In vitro reconstitution of MNIO enzymatic activity.*** The modification of Cys to 5-thiooxazole
254 is a new type of reaction catalysed by MNIO enzymes. To investigate the function of BufB1,
255 we purified recombinant SUMO-BufA1, BufB1 and BufC1 (Suppl. Fig. S8). Since MNIO
256 enzymes require Fe ions for activity (26, 29), BufB1 was analysed by inductively coupled
257 plasma - optical emission spectrometry, showing the presence of 2 Fe ions. Structural
258 alignments of a BufB1 model with the crystal structure of MbnB of *Vibrio caribbeanicus*, an
259 MNIO enzyme involved in methanobactin biosynthesis (26) confirmed that the Fe-coordinating
260 residues are conserved in BufB1. Next, BufA1 with the SUMO-tag cleaved was incubated with
261 BufB1 and/or BufC1 (Fig. 5A). LC-MS analyses showed that BufA1 was converted to a species
262 with a –8 Da mass shift only when both BufB1 and BufC1 were present (Fig. 5B; Suppl. Fig.
263 S9). Trypsin digestion of the *in vitro* modified BufA1 yielded the central 19-residue fragment
264 harbouring the thiooxazole groups derived from Cys^{II} and Cys^{III} as confirmed by MS/MS
265 analyses (Fig. 6B). Together with the gene inactivation data, these experiments established that
266 BufB1 and BufC1 are required and sufficient to install the PTMs on BufA1.
267
268 ***Signal peptide sequence is not essential for heterocycle formation***. The particularity of
269 bufferin biosynthesis is that BufA precursors harbour N-terminal Sec-dependent signal peptide
270 sequences. We investigated if this sequence is necessary for Cys transformation using the co-
271 expression system of His-SUMO-*bufA1* with *BufB1* and *BufC1* in *E. coli* (Extended Fig. 6).
272 The *bufA1* gene was mutated to generate variant precursors with the signal peptide truncated 8
273 residues from the N terminus (BufA1(-8aa)) or completely removed (BufA1(CP)).
274 Subsequently, LCMS analysis of the purified BufA1 after SUMO cleavage indicated that both
275 truncated precursors were modified with a 10 Da loss, consistent with the presence of two
276 thiooxazoles and one S-S bond (Extended Fig. 10). Of note, BufA1(CP) was converted by
277 BufB1/C1 in a less efficient manner, with the unmodified peptide also observed.

278

279 ***Large families of bufferin-like RiPPs in bacteria***. To determine how widespread bufferins are
280 among prokaryotes, we collected >14,000 MNIO enzyme-coding genes and found them to be
281 widely distributed among Proteobacteria, Terrabacteria, Myxococcota,
282 Fibrobacteres/Chlorobi/Bacterioidetes, Planctomycetes/Verrucomicrobia/Chlamydiota, and
283 Acidobacteriota groups (detailed *in silico* analyses will be published separately). We analysed
284 their genomic contexts and collected associated putative bufferin-like precursor genes to
285 perform sequence similarity network (SSN) analyses of the corresponding proteins. The largest
286 cluster corresponds to the DUF2282 family that includes *C. vibrioides* BufA1 (Fig. 6A). Most
287 of the other proteins have no family signature, but they contain conserved Cys residues,
288 consistent with their being potential RiPP precursors. BufA2 of *C. vibrioides* belongs to the
289 second largest family of proteins characterized by 6 or 12 conserved Cys residues, which we
290 named BUF_6/12Cys (Fig. 6A,B). Parallel SSN analyses of the MNIO enzymes superfamily
291 (Fig. 6C) showed that those associated with DF2282 or BUF_6/12Cys bufferins belong to the
292 largest sequence cluster, distinct from smaller clusters of enzymes involved in the biosynthesis
293 of methanobactins, RiPPs from *Chryseobacterium*, TglA-type pearlins and amino-pyruvatides
294 (24, 26-28, 30). Therefore, we have uncovered two large families of RiPPs whose biosynthesis
295 involves MNIO enzymes, exemplified by the *C. vibrioides* bufferins, that are distinct from
296 previously described MNIO enzyme-modified RiPPs.

297

298 ## Discussion

299 In this work, we unveiled the chemical nature and function of the products derived from heavy
300 metal-induced *gig*-like operons found in various environmental and pathogenic bacteria (16-
301 18). To the best of our knowledge, bufferins are the first genuine RiPP natural products
302 harbouring 5-thiooxazole motifs. Using model bufferin systems in *C. vibrioides*, we

303 demonstrated that the 5-thiooxazoles are key for copper binding. Peptide natural products with
304 other heterocycles are known to bind transition metals and fulfil different functions (2-5). Most
305 prominently, methanobactins scavenge copper from the milieu to feed it to cuproenzymes, and
306 some of them also protect bacteria from toxic metals such as mercury (44). The defensive role
307 of bufferins is reminiscent of those of the non-ribosomal siderophore peptides anthrochelin and
308 yersiniabactin, which can passivate copper by chelation (2, 45). However, the fate of copper
309 ions bound by bufferins remains unknown. Periplasmic bufferins might provide specific
310 metallochaperones with copper for delivery to cuproproteins or alternatively facilitate its
311 export.

312 We thus discovered yet another bacterial strategy of adaptation to copper that makes use of
313 such a new type of RiPPs widespread in the phylogenetic tree. Bufferins are part of complex
314 and interwoven metal defence systems in bacteria, as suggested by the fact that they do not
315 provide a high level of protection by themselves, as shown in *C. metallidurans* (17, 46). They
316 are probably best seen as additional players that buttress active defence systems through copper
317 passivation under specific environmental conditions. Nonetheless, their presence in pathogenic
318 bacteria indicates that they are likely beneficial to the latter in host-pathogen interactions, likely
319 by helping bacteria deal with copper encountered in eukaryotic phagocytes. Whether all
320 putative bufferins found by genome mining function in metal adaptation similar to our model
321 bufferins remain to be addressed. If so, the nature of the metals, the stoichiometry and the
322 affinity of the bufferins will likely depend on their primary and tertiary structures.

323 The biosynthesis of bufferins involves several novel features. Transformation of Cys to 5-
324 thiooxazole is catalysed by the MNIO BufB and its partner protein BufC. A similar reaction
325 was previously reported to engage radical-SAM enzymes (35). Intense efforts have been made
326 recently to explore the chemical space of RiPPs involving MNIOs (24, 25, 28, 30, 47). To date,
327 members of this superfamily of enzymes are known to catalyse remarkable oxidation reactions,

328 including oxazolone coupled to thioamide formation, excision of cysteine β-methylene, Cys-
329 involved macrocyclization, and C-C and C-N cleavages, as evidenced in the biosynthesis of
330 methanobactins, TglA-type pearlins, RiPPs in *Chryseobacterium*, aminopyruvatides, and
331 methanobactin-like peptides in *Vibrio*, respectively (24, 25, 27, 28, 30). This work thus further
332 expands the reaction spectrum of MNIOs. In line with previous work on Cys-modifying
333 MNIOs, BufB would similarly make use of the mixed-valent iron centres and proceed by an
334 intermediate step of proton abstraction from the Cβ of cysteine (26, 27, 29, 30) (Fig. 7).
335 Furthermore, bufferin precursor peptides commonly harbour signal peptides instead of leader
336 peptides at the N-terminus. Herein we showed that the signal peptide is dispensable for
337 heterocycle installation, which begs the question of the specific recognition between the
338 precursor and the BufB/C complex but highlights the biotechnological potential of BufB/C.
339 Our bioinformatic analyses indicated that bufferins currently represent the largest two
340 families of MNIO-associated RiPPs, widespread in different bacterial phyla. Putative bufferin
341 systems feature original properties, including the N-terminal signal peptides of their precursors
342 and the large sizes of their mature forms relative to most other RiPP precursor families. The
343 use of signal-peptides, which determine Sec-dependent export and signal-peptidase-mediated
344 processing of bufferins dispenses with the need for specific transporter and proteases genes in
345 their BGCs, possibly explaining why bufferins had previously been overlooked by genome
346 mining searches. The diversity in length and sequence of their cores provides almost infinite
347 possibilities to build new peptide metallophores.

348

349 **Methods**

350 ***C. vibrioides* constructs and growth conditions.** *C. vibrioides* NA1000 was used. Allelic
351 exchange was performed using pNPTS138 to construct deletion strains and to introduce
352 modified versions of *bufA1* and *bufA2*. pSRK-Km was used for expression of SigF. Plasmids

353 were mobilized from *E. coli* S17 into *C. vibrioides* by conjugation. The presence of the expected
354 deletions was verified by PCR. Chromosomal transcriptional fusions were generated using
355 pFUS2, and β-gal activities were measured as in (48). The plasmids, recombinant strains,
356 primers and synthetic genes used in this study are shown in Tables S4 to S6.

357 *C. vibrioides* was grown at 30°C in PYE medium with nalidixic acid (30 and 15 μg/ml in
358 solid and liquid medium, respectively), and kanamycin (20 and 5 μg/ml) or gentamycin (5 and
359 0.5 μg/ml) when carrying specific plasmids. To record growth curves, cultures in the stationary
360 phase were diluted to OD_{600} = 0.05 and inoculated in 96-well plates with continuous shaking at
361 30°C in a TECAN Spark plate reader, with OD_{600} measurements every 20 min for 28 h. $CuSO_4$
362 was added to 225 μM where indicated. The reporter strains were grown to early stationary phase
363 in the presence of metal ions or ROS at the indicated concentrations. Xanthine oxidase and
364 hypoxanthine were used to generate O_2^- and H_2O_2 (49). The production of ROS was quantified
365 using bacterial cultures grown for 24 h starting from OD = 0.1 at 30°C under moderate shaking.
366 The bacteria were then treated with 5 μM of CellROX Deep Red (Thermo fisher) for 30 min at
367 30°C, washed three times in 20 mM sodium phosphate (pH 7.5), and transferred into black-
368 bottom 96-wells plates. The emitted fluorescence was measured at 690 nm after excitation at
369 640 nm with a TECAN Spark plate reader. Biological quadruplicates were obtained in all
370 assays.

371 ***Genetic constructs in E. coli.*** pCA24 (50) was used for expression of the operon in *E. coli*. The
372 entire *bufI* operon was PCR-amplified from genomic DNA and inserted after the T5-lac
373 promoter of pCA24 using Gibson assembly (51). The sequence coding for BufA1 with a C-
374 terminal Strep-tag II was PCR-amplified and used to replace the native *bufA1* gene, yielding
375 pCA24-A^{str}BCD. For large-scale production of recombinant BufA1, the PCR-amplified gene
376 was inserted into SspI-linearized pETHisSUMO by ligase-independent cloning, generating
377 pETHisSUMO-A1. pACYC-Duet-based expression plasmids of N-terminally His_6-tagged

378 BufB1 and BufC1 were created using *in vivo* assembly (IVA) (52) yielding pACYC::HisC1
379 *and* pACYC::HisB1. For co-expression, *bufB1* was cloned into the MCS2 of pACYC::HisC1
380 by IVA cloning, yielding pACYC::HisC1B1Stag.

381 ***Gain-of function in E. coli.*** BL21(pCA24-*bufA1*^{str}*1BCD*) and BL21(pCA24-*psmCA*) (negative
382 control) (53) were grown overnight at 37°C, diluted 100-fold in M9 medium supplemented with
383 1xBME vitamin solution (Sigma), 0.5% glycerol, 34 µg/mL chloramphenicol and 1 mM IPTG
384 and grown at 37°C with vigorous shaking for 4 h. At OD_{600} = 0.1, one half of each culture was
385 exposed to 0.3 mM $CuSO_4$. Incubation was pursued for 3 h before CFUs were counted.

386 ***Amoeba experiments.*** Exponentially growing *C. vibrioides* cultures were concentrated to
387 OD_{600} = 1 in PYE medium and plated on PYE-agar with 1% glucose. 50-µL drops of
388 *Dictyostelium discoidum* grown to 80% confluency in HL/5 medium at 20°C and diluted to
389 10^6/mL were placed on the plate centres, before incubation at 20˚C for three days. ImageJ was
390 used to measure the densities of bacteria in the zones of contact between bacteria and amoeba,
391 divided by the area of these zones.

392 ***Native bufferin production and purification***. Cultures of $Cv_{buf1}^{TwStrep}$(pSigF),
393 Cvbuf1^{6His}(pSigF) and Cvbuf2^{6His}(pSigF) were started at OD_{600} = 0.1 in PYE supplemented
394 with 100 µM IPTG. Bacteria were harvested after overnight growth, resuspended in 100 mM
395 Tris-HCl (pH = 8), 150 mM NaCl and broken using a French press. Buf1^{TwStrep} was purified
396 from the clarified lysate using a 1-mL StrepTrap XT column (Cytiva) following the
397 manufacturer's instructions, concentrated using an Amicon ultrafiltration device and dialysed
398 against 25 mM Hepes (pH 8) 150 mM NaCl. Buf1^{twstr} was truncated *in vivo* just after the first
399 strep tag motif, as evidenced by native MS. The Buf1^{6His} and Buf2^{6His} proteins were purified on
400 1-mL Ni^{2+} columns using standard procedures.

401 For purification of isotopically labeled BufA1, *E. coli* BL21(pCA-A^{str}BCD) was grown in
402 in M9 medium supplemented with 34 µg/mL chloramphenicol, 1xBME vitamin solution

403 (Sigma), 0.5% glycerol-$^{13}C_3$ and 0.1 g/L $^{15}NH_4Cl$ at 37 °C until OD600 ~ 0.6. Protein
404 expression was induced with 1 mM IPTG, and the culture continued at 22°C overnight. $CuSO_4$
405 was added to 0.3 mM following overnight growth, and after 4 more hours bacteria were
406 harvested by centrifugation. They were resuspended in 50 mM Tris-HCl buffer (pH 8.0), 300
407 mM NaCl and lysed by sonication. The clarified lysate was applied to a 1-mL Strep-Tactin®
408 Superflow column (IBA Lifesciences, Germany), and after washing with 20 column volumes
409 of the same buffer, $BufA^{str}$ was eluted with 2.5 mM desthiobiotin, 50 mM Na-phosphate buffer
410 (pH 7.0), 50 mM NaCl. The molar extinction coefficient used for $Buf1^{str}$ was 38,158 $M^{-1}cm^{-1}$.
411 ***Protein production and purification for in vitro assays.*** N-His_6-BufB1 and N-His_6-BufC1
412 were each produced in *E. coli* BL21(DE3), in 1 L autoinduction ZYM-5052 medium (54)
413 supplemented with 250 µM ferrous ammonium sulphate for BufB1. After 4 h of growth at 37°C,
414 the temperature was lowered to 18°C and cultures were pursued for 16 h. N-His_6-tagged
415 SUMO-BufA1 was produced in 1 L TB medium, with bacteria grown until OD_{600} = 0.6-0.7
416 before cooling down on ice. After adding IPTG to 0.1 mM, the cultures were pursued at 18°C
417 for 16 h. Bacteria were resuspended in 50 mM Tris-HCl (pH 7.6), 300 mM NaCl, 10% glycerol,
418 10 mM imidazole, and lysed using French Press or by sonication in the case of BufA1.
419 Recombinant proteins were purified by gravity using a 5-mL-column packed with Ni-NTA
420 resin (Qiagen). After washes with 30 mM and 60 mM imidazole in 50 mM Tris-HCl (pH 7.6),
421 300 mM NaCl, the proteins were eluted with 50 mM Tris-HCl (pH 7.6), 300 mM NaCl, 250
422 mM imidazole, concentrated by ultrafiltration using Amicon centrifugal units, and buffer
423 exchanged by PD10 columns (Cytiva) to 50 mM Tris-HCl (pH 7.6), 150 mM NaCl, 20%
424 glycerol. Purified proteins were flash frozen and stored at -80°C. Purification followed the same
425 procedure for all three proteins except that 10 mM of Tris(2-carboxyethyl)phosphine
426 hydrochloride was added to all buffers for BufA1. The iron content of His_6-BufB1 was
427 measured by using an inductively coupled plasma - optical emission spectrometer (ICP-OES

428 5110 VDV, Agilent Technologies) at λ = 238.204 nm calibrated using standard solutions. All
429 the solutions were acidified with HNO_3 (Fisher Scientific, 67–69%, Optima and trace metal
430 grade). Certified water Enviromat (SCP, N°140-025-038) was analysed for quality control
431 (certified value of 0.581 +/- 0.011 mg/L, experimental result of 0.59 +/- 0.02 mg/L). The limit
432 of detection was estimated to 0.005 mg/L and the average blank value was below this limit.
433 ***Large-scale production of SUMO-BufA1 for NMR studies.*** *E. coli* BL21(DE3,
434 pACYC::HisC1B1Stag, pETHisSUMO-A1) was grown in 2 L TB medium. For ^{13}C and ^{15}N-
435 labelling, protein expression was carried out in 1 L M9 medium supplemented with 1 g/L of
436 ^{13}C-glucose and 5 g/L $^{15}NH_4Cl$. In both cases, cultures were grown until OD_{600} = 0.6-0.7 before
437 cooling down on ice. After adding ITPG to 0.1 mM, the cultures were pursued at 18°C for 16
438 h (TB medium) or 48 h (M9 medium), respectively. Purification of modified N-His_6-tagged
439 SUMO-BufA1 was performed as described above.
440 ***Peptide analyses by MS.*** Cell pellets and culture supernatants from 25-mL overnight *C.*
441 *vibrioides* cultures were resuspended in 1 mL 50 mM Tris HCl (pH 7.5) and submitted to fast-
442 prep lysis in Lysing Matrix B tubes (force 5, 30 sec, 2 times). The clarified lysates were
443 submitted to solid-phase extraction (SPE) on Sep-Pak tC2 Plus Light Cartridges (Waters)
444 conditioned with 5 mL methanol and 5 mL 0.01 % formic acid (FA). The cartridges were
445 washed with 5 mL 0.01 % FA and eluted with 2 mL methanol. The eluted fractions were split
446 in two, evaporated under vacuum and dissolved in 50 µL 0.01% FA/methanol 1:1 (v/v). One
447 was left intact (I), and the other was treated with 10 mM dithiothreitol (DTT) for 1 h at 50°C
448 and alkylated with 15 mM iodoacetamide for 1 h at 20°C in the dark. Half of that solution was
449 collected (R1) and the other half was treated with 0.01 µg/µL trypsin (Gold, Promega) overnight
450 at 37°C (R2). Alternatively, reduction-alkylation was performed using DTT together with 2-
451 bromoethylamine (55). R1 and R2 were desalted using Pierce C18 Spin columns. The purified
452 $Buf1^{twstr}$ was analysed by LC-MS directly or after reduction-alkylation and digestion with

453 trypsin as above. I, R1 and R2 were analysed by ultra-high-performance liquid
454 chromatography-MS on an Ultimate 3000-RSLC system (Thermo Scientific) connected to an
455 electrospray ionization- quadrupole–time of flight instrument (Maxis II ETD, Bruker
456 Daltonics). The separation was achieved using an Aeris widepore C4 column (3.6 µm, 200 Å,
457 2.1 × 100 mm, Phenomenex) for I and R1 samples and a RSLC Polar Advantage II Acclaim
458 column (2.2 µm, 120 Å, 2.1 × 100 mm, Thermo Scientific) for R2, with a linear gradient (2-80 %
459 in 15 min) of mobile phases A (FA 0.1%) and B (LC-MS grade acetonitrile (ACN) + FA
460 0.08%), at 300 µL/min. For I and R1, LC-MS detection was carried out in positive mode in the
461 range *m/z* 250-2500. For R2 samples, data-dependent LCMS/MS acquisitions were conducted.
462 They were also analyzed by nanoLC-MS on an UltiMate 3000 RSLCnano System coupled to
463 an Orbitrap Fusion Lumos Tribrid (Thermo Fisher Scientific). The separation was achieved
464 using a C18 Biosphere column (2 µm, 75 µm × 500 mm Neo Thermoscientific) with a linear
465 gradient (2.5-45% B for 55 min, 45-98% for 10 min and 2.5% for 10 min) of phases A (FA
466 0.1%/ACN 98/2) and B (FA 0.1%/ACN 20/80) at 0.250 µL/min. The mass spectrometer was
467 operated in positive mode in the range *m/z* 150-1200. Data-dependent LCMS/MS acquisition
468 mode was used. Full MS scans were captured with a resolution of 120,000. Peptide
469 identification was performed using X!TandemPipeline (56) or PEAKS Studio X Pro
470 (Bioinfomatics Solutions Inc.), against the *Caulobacter* UniProtKB database (version 2023)
471 with the following parameters set as variable modifications: one possible missed cleavage, Cys
472 carboxyamidomethylation, and Met oxidation. Precursor mass and fragment mass tolerance
473 were 10 ppm and 0.02 Da, respectively. Data filtering was achieved according to a peptide E
474 value < 0.05. The false discovery rate at the peptide level was assessed from searches against a
475 decoy database. MS2 spectra were analysed using BYONIC™ (Protein Metrics) together with
476 i2MassChroQ 0.6.7 (http://pappso.inrae.fr/bioinfo/i2masschroq) and SpecGlobTool to
477 highlight and localize unknown PTMs (34).

478 Native MS was carried out using flow injection with 50 µL/min 10 mM ammonium
479 acetate (pH 7). One µL of purified peptide at 20 µM in 10 mM ammonium acetate (pH 7) was
480 injected. For *in vitro* binding experiments, the peptide was previously incubated for 1 h with
481 $CuCl_2$ (1 or 2 equivalents) at room temperature.
482 ***NMR analyses.*** Purified His-SUMO-BufA1* was incubated with trypsin (1:100 w/w) at 37°C
483 overnight in 50 mM Tris-HCl (pH 7.6), 10 mM TCEP. Purification of the 19-residue central
484 trypsin fragment containing two modified Cys residues was conducted by HPLC (UltiMate™
485 3000 System, Thermo Scientific) on a preparative C18 column (Luna C18 (2), 5 µm, 100 Å,
486 250 x 10 mm, Phenomenex) at ambient temperature. Separation was performed using a linear
487 gradient (6 min at 5% B, 6-14 min from 5-30 % B, 14-18 min to 80% B, and 18-22 min at
488 80%B) of mobile phases A (0.1% FA) and B (ACN) at 3 mL/min, and monitored at 280 and
489 305 nm. Fractions containing the relevant peptide were pooled and dried by SpeedVac. A
490 sample of 3.4 mg of the tryptic peptide dissolved in 550 µL of 50 mM Na phosphate buffer (pH
491 6.5), 150 mM NaCl, with 25 µL D_2O and Trimethyl Silyl Propionate (TSP) as reference was
492 introduced in a standard 5-mm NMR tube. All spectra were recorded at 293 K on an 800-MHz
493 NEO Bruker spectrometer equipped with a QCP cryogenic probe head. TOCSY and ROESY
494 spectra were recorded for assignment of the peptide with 16 k x 512 points for a spectral width
495 of 12 ppm in both dimensions, with 16 and 64 scans per increment, respectively (total
496 measurement times of 4 h and 16 h, respectively). Scalar coupling transfer was accomplished
497 during a 60-ms DIPSI2 mixing time, whereas a 100-ms spin lock was used for the dipolar
498 magnetization transfer. The relaxation delay was set to 1 s for both spectra. The natural
499 abundance ^{1}H, ^{15}N HSQC spectrum was recorded with the Bruker hsqcf3gpph19 pulse
500 program, with 2 k x 128 points for a spectral width of 12 ppm x 36 ppm, centered on 4.7 ppm
501 and 119 ppm for the H and the N dimensions, respectively, and 256 scans per increment. Natural
502 abundance ^{1}H, ^{13}C HSQC and HMBC spectra were recorded with standard Bruker pulse

503 programs (hsqcetgpsisp.2 and hmbcedetgpl3nd), with 2 k x 256 points for a spectral window of
504 12 x 40 ppm and the ^{13}C carrier set at 80 ppm, and with 2 k x 256 points for a spectral window
505 of 12 x 140 ppm and the ^{13}C window centered at 100 ppm, respectively, and 64 scans per
506 increment for both. A HNCACB spectrum was recorded on the ^{15}N, ^{13}C labeled peptide as a
507 cube of 12 x 30 x 70 ppm sampled with 2 k x 76 x 256 points centered at 4.7 x 119 x 70 ppm
508 in the ^{1}H, ^{15}N and ^{13}C dimensions, respectively. For the HNCO spectrum, the ^{13}C carrier was
509 shifted to 175 ppm, and the ^{13}CO window of 30 ppm was sampled with 64 points. In order to
510 estimate the carbonyl frequencies of the modified Cys residues, we recorded the H(N)CO planes
511 of the latter spectrum while introducing a selective pulse with varying offset during the ^{13}CO
512 evolution period.

513 ***EPR experiments.*** Pulsed (EDFS) EPR experiments on the *in vivo*-formed Buf1^{twstr}-copper
514 complex (200 μM) were carried out using an ELEXSYS E-580 spectrometer (Bruker) equipped
515 with a Super-Q FTu bridge for X- (9 GHz) and Q- (35 GHz) band experiments. Samples were
516 drawn into 3 × 4 mm quartz tubes, flash-frozen into liquid nitrogen and rapidly transferred into
517 precooled dielectric resonators, ER 4118X-MD5W X-band and ER 5106QT-2w Q-band. Both
518 X- and Q-band spectra were acquired at 20 K using a Bruker Cryogen-free (Cold-Edge) cooling
519 system. Microwave pulse lengths $t_{\pi/2}$ = 10-12 ns (Q-band) and $t_{\pi/2}$ = 16 ns (X-band) were used
520 with inter-pulse delays of τ = 172 ns (Q-band) and τ = 132 ns (X-band). A two-step phase-cycle
521 was applied to remove all unwanted echoes on EDFS. Numerical simulation of the EPR spectra
522 was conducted using the Matlab toolbox Easyspin 5.2.35.

523 ***Spectrophotometric copper binding assay***. Copper binding to purified Buf1^{twstr} was assayed
524 using competition experiments using a complex between 4-(2-pyridylazo)resorcinol (PAR) and
525 Cu^{2+} (ε_{505nm} =41,500 M^{-1} cm^{-1}) (42), with 4 μM Cu, 10 μM PAR and 5 to 40 μM Buf1^{twstr}. The
526 visible spectra were recorded after increasing incubation periods at room temperature.

527 ***Enzymatic assays in vitro***. Standard reactions were carried out in 100-µl solutions of 50 µM
528 purified His-SUMO-BufA1 in 50 mM Tris-HCl (pH 7.6) and 10 mM TCEP. For removal of the
529 affinity tag, this mixture was first incubated with in-house purified SUMO protease at a 1:20
530 ratio of protease/peptide overnight at 4°C. Subsequently, either or both purified N-His_6-BufB1
531 (25 µM) and N-His_6-BufC1 (25 µM) were added, and the mixtures were incubated at 30°C for
532 16 h. For control reactions BufB1 and BufC1 were inactivated by heating. Half of the reaction
533 mixture was desalted using Zeba spin columns (Thermo Fisher Scientific) and directly analysed
534 by LC-MSMS on a Aeris widepore C4 column. The other half was treated with trypsin
535 (Promega) added to 1:100 (w/w) and incubated for 3 h at 37°C before LC-MSMS analysis on
536 a RSLC Polar Advantage II Acclaim column. LC-MSMS measurements were performed on an
537 Ultimate 3000-RSLC system (Thermo Scientific) connected to a high-resolution ESI-Q-TOF
538 mass spectrometer (Maxis II ETD, Bruker Daltonics), as described above.
539 ***In silico analyses.*** The non-redundant NCBI database (release of Jan 2023) was searched for
540 MNIO-coding genes. To identify new families of RiPPs, a script was designed to collect genes
541 next to and in the same orientation as MNIO genes, coding for proteins less than 200 residues
542 long. Predictions of signal peptides were performed using various softwares (Scotopus, Philius,
543 Octopius, Scampi, Polyphobius, Topcons). Analyses by the Enzyme Function Initiative -
544 Enzyme Similarity Tool (EFI-EST) were carried out with the predicted proteins (after removal
545 of their signal peptides) to build sequence similarity networks (SSN). For the generation of a
546 hmm profile for the BUF_6/12Cys family, the procedure described in (57) was followed.
547 Briefly, a few dozen proteins were picked from the cluster of interest of the Representative
548 Node Network, and their sequences were aligned with MAFFT (L-INS-i). After manual editing
549 of the non-conserved mostly N- and C-terminal regions, a hmm profile was generated using
550 this seed alignment.

551

552 **References**

553 1. Li Y, Rebuffat S. The manifold roles of microbial ribosomal peptide-based natural products in
554 physiology and ecology. J Biol Chem. 2020;295(1):34-54.

555 2. Büttner H, Hörl J, Krabbe J, Hertweck C. Discovery and biosynthesis of anthrochelin, a growth-
556 promoting metallophore of the human pathogen *Luteibacter anthropi*. ChemBioChem.
557 2023;24:e202300322.

558 3. Chaturvedi KS, Hung CS, Crowley JR, Stapleton AE, Henderson JP. The siderophore yersiniabactin
559 binds copper to protect pathogens during infection. Nat Chem Biol. 2012;8(8):731-6.

560 4. Ghssein G, Brutesco C, Ouerdane L, Fojcik C, Izaute A, Wang S, et al. Biosynthesis of a broad-
561 spectrum nicotianamine-like metallophore in Staphylococcus aureus. Science. 2016;352(6289):1105-9.

562 5. Kenney GE, Rosenzweig AC. Chalkophores. Annu Rev Biochem. 2018;87:645-76.

563 6. Andrei A, Ozturk Y, Khalfaoui-Hassani B, Rauch J, Marckmann D, Trasnea PI, et al. Cu Homeostasis
564 in Bacteria: The Ins and Outs. Membranes (Basel). 2020;10(9).

565 7. Solioz M. Copper and Bacteria. Evolution, homeostasis and toxicity. Springer, editor. Cham,
566 Switzerland: Springer Nature Switzerland AG; 2018.

567 8. Macomber L, Imlay JA. The iron-sulfur clusters of dehydratases are primary intracellular targets of
568 copper toxicity. Proc Natl Acad Sci U S A. 2009;106(20):8344-9.

569 9. Zuily L, Lahrach N, Fassler R, Genest O, Faller P, Seneque O, et al. Copper Induces Protein
570 Aggregation, a Toxic Process Compensated by Molecular Chaperones. mBio. 2022:e0325121.

571 10. Hao X, Luthje F, Ronn R, German NA, Li X, Huang F, et al. A role for copper in protozoan grazing
572 - two billion years selecting for bacterial copper resistance. Mol Microbiol. 2016;102(4):628-41.

573 11. Sheldon JR, Skaar EP. Metals as phagocyte antimicrobial effectors. Curr Opin Immunol. 2019;60:1-9.

574 12. Arguello JM, Raimunda D, Padilla-Benavides T. Mechanisms of copper homeostasis in bacteria. Front
575 Cell Infect Microbiol. 2013;3:73.

576 13. Chandrangsu P, Rensing C, Helmann JD. Metal homeostasis and resistance in bacteria. Nat Rev
577 Microbiol. 2017;15(6):338-50.

578 14. Hodgkinson V, Petris MJ. Copper homeostasis at the host-pathogen interface. J Biol Chem.
579 2012;287(17):13549-55.

580 15. Coutte L, Antoine R, Slupek S, Solans L, Derop J, Bonnefond A, et al. Combined RNAseq and
581 ChIPseq Analyses of the BvgA Virulence Regulator of Bordetella pertussis. mSystems. 2020;5(3).

582 16. Jwanoswki K, Wells C, Bruce T, Rutt J, Banks T, McNealy TL. The Legionella pneumophila GIG
583 operon responds to gold and copper in planktonic and biofilm cultures. PLoS One.
584 2017;12(5):e0174245.

585 17. Kohler C, Lourenco RF, Avelar GM, Gomes SL. Extracytoplasmic function (ECF) sigma factor
586 sigmaF is involved in Caulobacter crescentus response to heavy metal stress. BMC Microbiol.
587 2012;12:210.

588 18. Wiesemann N, Mohr J, Grosse C, Herzberg M, Hause G, Reith F, et al. Influence of copper resistance
589 determinants on gold transformation by Cupriavidus metallidurans strain CH34. J Bacteriol.
590 2013;195(10):2298-308.

591 19. Maertens L, Cherry P, Tilquin F, Van Houdt R, Matroule JY. Environmental Conditions Modulate the
592 Transcriptomic Response of Both Caulobacter crescentus Morphotypes to Cu Stress. Microorganisms.
593 2021;9(6).

20. Arnison PG, Bibb MJ, Bierbaum G, Bowers AA, Bugni TS, Bulaj G, et al. Ribosomally synthesized and post-translationally modified peptide natural products: overview and recommendations for a universal nomenclature. Nat Prod Rep. 2013;30(1):108-60.

21. Montalban-Lopez M, Scott TA, Ramesh S, Rahman IR, van Heel AJ, Viel JH, et al. New developments in RiPP discovery, enzymology and engineering. Nat Prod Rep. 2021;38(1):130-239.

22. Burkhart BJ, Hudson GA, Dunbar KL, Mitchell DA. A prevalent peptide-binding domain guides ribosomal natural product biosynthesis. Nat Chem Biol. 2015;11(8):564-70.

23. Chekan JR, Ongpipattanakul C, Nair SK. Steric complementarity directs sequence promiscuous leader binding in RiPP biosynthesis. Proc Natl Acad Sci U S A. 2019;116(48):24049-55.

24. Ayikpoe RS, Zhu L, Chen JY, Ting CP, van der Donk WA. Macrocyclization and Backbone Rearrangement During RiPP Biosynthesis by a SAM-Dependent Domain-of-Unknown-Function 692. ACS Cent Sci. 2023;9(5):1008-18.

25. Chioti VT, Clark KA, Ganley JG, Han EJ, Seyedsayamdost MR. N-Calpha Bond Cleavage Catalyzed by a Multinuclear Iron Oxygenase from a Divergent Methanobactin-like RiPP Gene Cluster. J Am Chem Soc. 2024.

26. Dou C, Long Z, Li S, Zhou D, Jin Y, Zhang L, et al. Crystal structure and catalytic mechanism of the MbnBC holoenzyme required for methanobactin biosynthesis. Cell Res. 2022;32(3):302-14.

27. Kenney GE, Dassama LMK, Pandelia ME, Gizzi AS, Martinie RJ, Gao P, et al. The biosynthesis of methanobactin. Science. 2018;359(6382):1411-6.

28. Nguyen DT, Zhu L, Gray DL, Woods TJ, Padhi C, Flatt KM, et al. Biosynthesis of macrocyclic peptides with C-terminal beta-amino-alpha-keto acid groups by three different metalloenzymes. BioRxiv. 2024.

29. Park YJ, Jodts RJ, Slater JW, Reyes RM, Winton VJ, Montaser RA, et al. A mixed-valent Fe(II)Fe(III) species converts cysteine to an oxazolone/thioamide pair in methanobactin biosynthesis. Proc Natl Acad Sci U S A. 2022;119(13):e2123566119.

30. Ting CP, Funk MA, Halaby SL, Zhang Z, Gonen T, van der Donk WA. Use of a scaffold peptide in the biosynthesis of amino acid-derived natural products. Science. 2019;365(6450):280-4.

31. Müller FH, Bandeiras TM, Urich T, Teixeira M, Gomes CM, Kletzin A. Coupling of the pathway of sulphur oxidation to dioxygen reduction: characterization of a novel membrane-bound thiosulphate:quinone oxidoreductase. Mol Microbiol. 2004;53(4):1147-60.

32. Nambi S, Long JE, Mishra BB, Baker R, Murphy KC, Olive AJ, et al. The Oxidative Stress Network of Mycobacterium tuberculosis Reveals Coordination between Radical Detoxification Systems. Cell Host Microbe. 2015;17(6):829-37.

33. Alvarez-Martinez CE, Baldini RL, Gomes SL. A caulobacter crescentus extracytoplasmic function sigma factor mediating the response to oxidative stress in stationary phase. J Bacteriol. 2006;188(5):1835-46.

34. Prunier G, Cherkaoui M, Lysiak A, Langella O, Blein-Nicolas M, Lollier V, et al. Fast alignment of mass spectra in large proteomics datasets, capturing dissimilarities arising from multiple complex modifications of peptides. BMC Bioinformatics. 2023;24(1):421.

35. Lewis JK, Jochimsen AS, Lefave SJ, Young AP, Kincannon WM, Roberts AG, et al. New Role for Radical SAM Enzymes in the Biosynthesis of Thio(seleno)oxazole RiPP Natural Products. Biochemistry. 2021;60(45):3347-61.

36. Wüthrich K. NMR of proteins and nucleic acids. New York: Wiley; 1986.

37. Sattler M. Heteronuclear multidimensional NMR experiments for the structure determination of proteins in solution employing pulsed field gradients. Progr Nucl Magn Reson Spectr. 1999;34:93-158.

639 38. Yamazaki T, Lee W, Arrowsmith CH, Muhandiram DR, Kay LE. A Suite of Triple Resonance NMR
640 Experiments for the Backbone Assignment of 15N, 13C, 2H Labeled Proteins with High Sensitivity. J
641 Am Chem Soc 1994;116:11655-66.

642 39. Fiore KE, Patist MJ, Giannakoulias S, Huang CH, Verma H, Khatri B, et al. Structural impact of
643 thioamide incorporation into a beta-hairpin. RSC Chem Biol. 2022;3(5):582-91.

644 40. Wishart DS, Bigam CG, Holm A, Hodges RS, Sykes BD. 1H, 13C and 15N random coil NMR chemical
645 shifts of the common amino acids. I. Investigations of nearest-neighbor effects. J Biomol NMR.
646 1995;5(1):67-81.

647 41. NMR spectroscopy - Hans Reich NMR collection - content.

648 42. Novoa-Aponte L, Xu C, Soncini FC, Arguello JM. The Two-Component System CopRS Maintains
649 Subfemtomolar Levels of Free Copper in the Periplasm of Pseudomonas aeruginosa Using a
650 Phosphatase-Based Mechanism. mSphere. 2020;5(6).

651 43. Bennett B, Kowalski JM. EPR Methods for Biological Cu(II): L-Band CW and NARS. Methods
652 Enzymol. 2015;563:341-61.

653 44. Baral BS, Bandow NL, Vorobev A, Freemeier BC, Bergman BH, Herdendorf TJ, et al. Mercury binding
654 by methanobactin from Methylocystis strain SB2. J Inorg Biochem. 2014;141:161-9.

655 45. Koh EI, Robinson AE, Bandara N, Rogers BE, Henderson JP. Copper import in Escherichia coli by
656 the yersiniabactin metallophore system. Nat Chem Biol. 2017;13(9):1016-21.

657 46. Hirth N, Gerlach MS, Wiesemann N, Herzberg M, Grosse C, Nies DH. Full Copper Resistance in
658 Cupriavidus metallidurans Requires the Interplay of Many Resistance Systems. Appl Environ
659 Microbiol. 2023;89(6):e0056723.

660 47. Clark KA, Seyedsayamdost MR. Bioinformatic Atlas of Radical SAM Enzyme-Modified RiPP Natural
661 Products Reveals an Isoleucine-Tryptophan Crosslink. J Am Chem Soc. 2022;144(39):17876-88.

662 48. Antoine R, Alonso S, Raze D, Coutte L, Lesjean S, Willery E, et al. New virulence-activated and
663 virulence-repressed genes identified by systematic gene inactivation and generation of transcriptional
664 fusions in Bordetella pertussis. J Bacteriol. 2000;182(20):5902-5.

665 49. Rivera-Millot A, Slupek S, Chatagnon J, Roy G, Saliou JM, Billon G, et al. Streamlined copper defenses
666 make Bordetella pertussis reliant on custom-made operon. Commun Biol. 2021;4(1):46.

667 50. Kitagawa M, Ara T, Arifuzzaman M, Ioka-Nakamichi T, Inamoto E, Toyonaga H, et al. Complete set
668 of ORF clones of Escherichia coli ASKA library (a complete set of E. coli K-12 ORF archive): unique
669 resources for biological research. DNA Res. 2005;12(5):291-9.

670 51. Baba T, Ara T, Hasegawa M, Takai Y, Okumura Y, Baba M, et al. Construction of Escherichia coli K-
671 12 in-frame, single-gene knockout mutants: the Keio collection. Mol Syst Biol. 2006;2:2006 0008.

672 52. Garcia-Nafria J, Watson JF, Greger IH. IVA cloning: A single-tube universal cloning system exploiting
673 bacterial In Vivo Assembly. Sci Rep. 2016;6:27459.

674 53. Zyubko T, Serebryakova M, Andreeva J, Metelev M, Lippens G, Dubiley S, et al. Efficient in vivo
675 synthesis of lasso peptide pseudomycoidin proceeds in the absence of both the leader and the leader
676 peptidase. Chem Sci. 2019;10(42):9699-707.

677 54. Studier FW. Protein production by auto-induction in high density shaking cultures. Protein Expr Purif.
678 2005;41(1):207-34.

679 55. Serra A, Hemu X, Nguyen GK, Nguyen NT, Sze SK, Tam JP. A high-throughput peptidomic strategy
680 to decipher the molecular diversity of cyclic cysteine-rich peptides. Sci Rep. 2016;6:23005.

681 56. Langella O, Valot B, Balliau T, Blein-Nicolas M, Bonhomme L, Zivy M. X!TandemPipeline: A Tool
682 to Manage Sequence Redundancy for Protein Inference and Phosphosite Identification. J Proteome
683 Res. 2017;16(2):494-503.

57. Shelton KE, Mitchell DA. Bioinformatic prediction and experimental validation of RiPP recognition elements. Methods Enzymol. 2023;679:191-233.

Acknowledgments. We thank J.-M. Saliou for preliminary MS analyses and J.-Y. Matroule and P. Cherry for providing *C. vibrioides* strains, plasmids and protocols. This project was funded by the ANR grant CuRiPP (ANR-22-CE44-0001-02) to FJD. L. Leprevost was supported by a doctoral fellowship of Lille University. S. Jünger was supported by a PhD fellowship of the French Ministry of Education (ED 227 MNHN-SU). For the EPR experiments the financial support from the IR INFRANALYTICS FR2054 is acknowledged. ICP-OES measurements were performed by V. Alaimo on the Chevreul Institute Platform (U-Lille / CNRS). The Region Hauts de France and the French government are acknowledged for funding this apparatus.

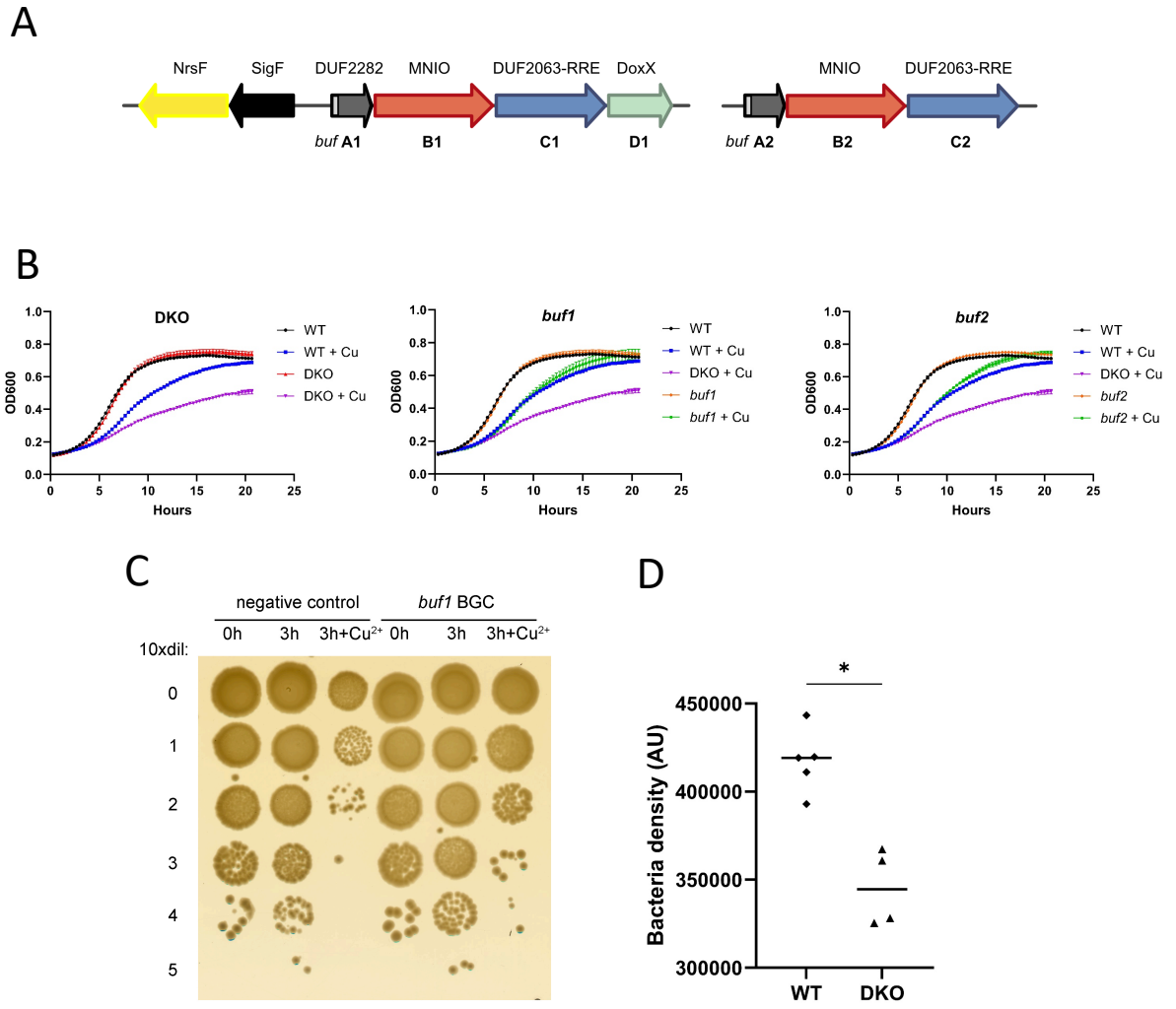

Fig. 1. Biosynthetic gene clusters and functions of bufferins. A. Gene composition of the *buf1* and *buf2* BGCs. The signal peptide-coding sequences and core sequences of the *bufA1* and *bufA2* genes are shown in pale and dark grey, respectively. In anti-sense of *buf1ABCD* are genes coding for the extracellular-type sigma factor SigF and the anti-sigma factor NrsF that regulate the expression of *buf1* and *buf2*. B. Effect of copper on bacterial growth. The Cv_{DKO}, $Cv_{buf1ABCD}$ (denoted *buf1)* and $Cv_{buf2ABC}$ (denoted *buf2*) strains were grown in liquid PYE medium without or with 225 µM copper. Their growth was measured in biological quadruplicates. C. Gain-of-function in *Escherichia coli*. Expression of *buf1* in *E. coli* BL21(pCA24-buf1A^{str}BCD) was induced by IPTG, and the bacteria were challenged with 0.3 mM CuSO4 for three hours before serial dilutions. BL21(pCA24-psmCA) expressing a non-relevant lasso peptide BGC was used as a negative control. D. Assay of bacterial lysis by *D. discoidum*. Bacterial densities of the lysis plaques were determined using ImageJ analyses. A non parametric Mann-Whitney test (two-sided) was used to analyze the differences between the Cv_{WT} strain (n=5) and the Cv_{DKO} strain (n=4). A P value of 0.05 was considered statistically significant (* indicates p = 0.0159). The medians are shown (WT = 419,226 and DKO = 344,516) with a confidence interval of 96.83%. The ranks calculated were WT = 35 and DKO = 10.

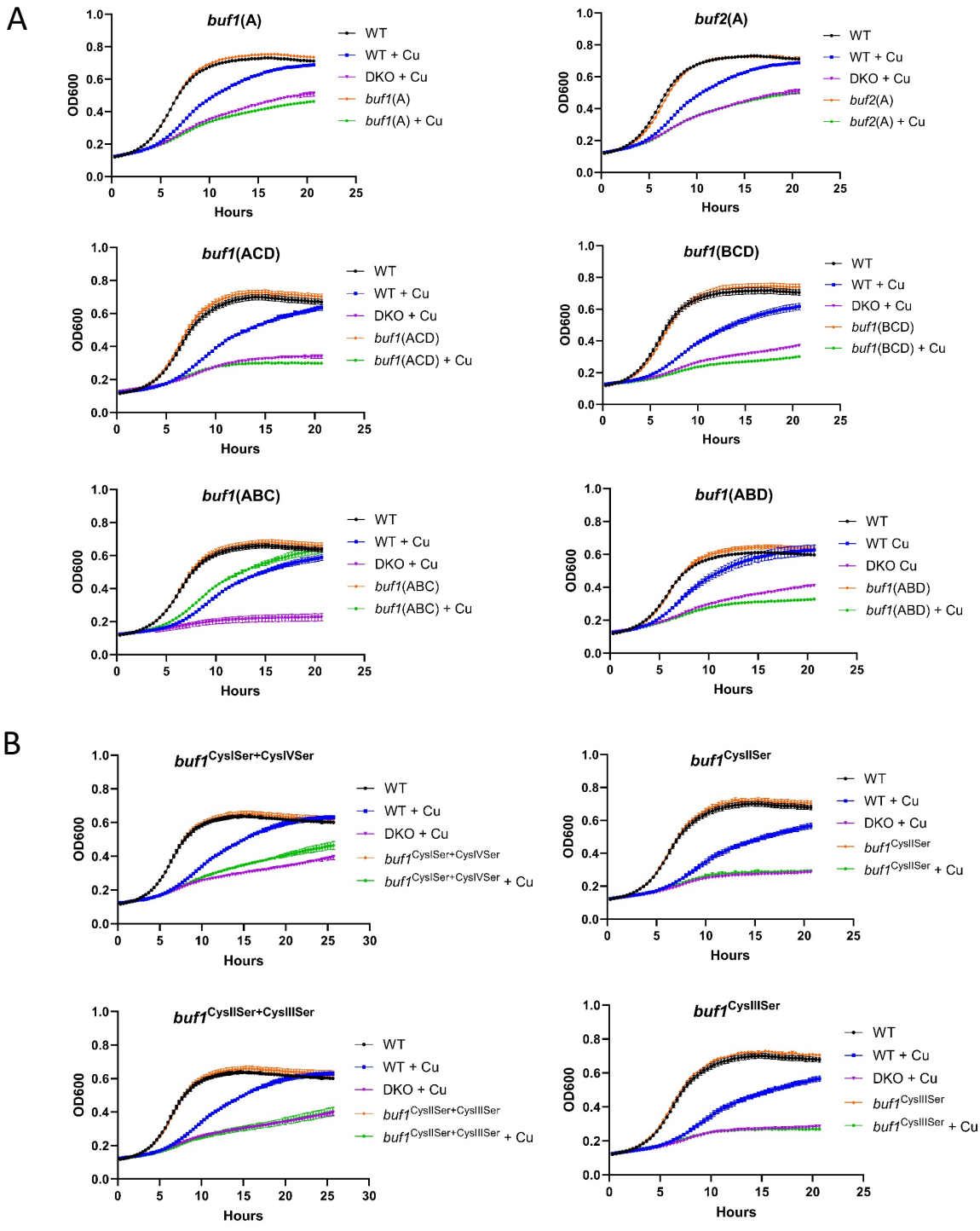

Fig. 2. Effect of Cu on the growth of *C. vibrioides*. A. Strains that express the indicated genes were grown in PYE medium or in PYE medium containing 225 uM copper. All deletions were performed in strains carrying a single *buf* BGC. B. Strains expressing the entire *buf1* BGC with the indicated substitutions in BufA1 were grown with or without copper as in A.

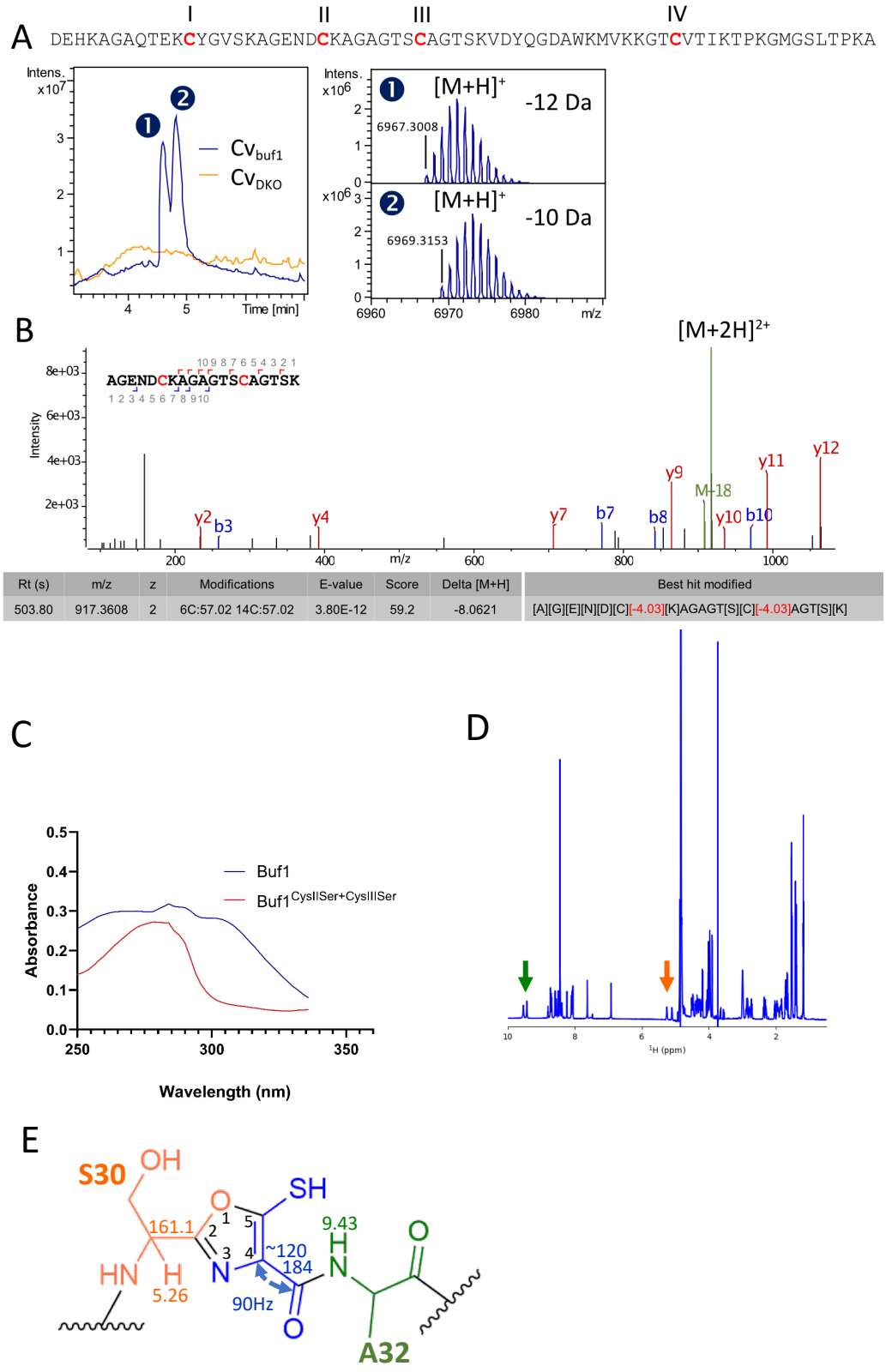

Fig. 3. Post-translational modifications on Bufferin 1. A. Sequence of Buf1 with the Cys residues labelled I to IV, and top-down LC-MS analyses of cell extracts of Cv_{buf1}(pSigF) compared with Cv_{DKO}(pSigF). Left panel: total ion chromatograms, right panels: deconvoluted mass spectra of the two compounds detected only for Cv_{buf1}(pSigF). Their molecular weights correspond to the core peptide (i.e. after removal of the signal peptide; calculated monoisotopic Mw=6978.35 Da), with mass shifts of -10 Da ($[M+H]^+$ at *m/z* 6969.32) and -12 Da ($[M+H]^+$ at *m/z* 6967.30). B. Bottom-up analysis of Buf1. MS/MS spectrum of the central tryptic peptide ($[M+2H]^{2+}$ at *m/z* 917.36). The two Cys carry carbamidomethyl groups resulting from alkylation with iodoacetamide (+ 57.02 Da), together with -4.03 Da mass shifts. C. UV-visible spectra of purified Buf1 and $Buf1^{CysIISer+CysIIISer}$. The broad absorbance band beyond 290 nm for the wt peptide suggests the presence of heterocycle(s) that are absent in the mutant peptide. D. ^{1}H NMR spectrum of the central tryptic peptide. Anomalous resonances are indicated by orange and green arrows. E. Tripeptide centered on Cys31 (= Cys^{III}) modified into a thio-oxazole. The values of the chemical displacements (in ppm) are given for various atoms. Salient NMR parameters leading to this assignment are the downfield shifted Hα proton of Ser30 (5.26 ppm, orange arrow in D), the ^{13}C assignments of 161.6 and 120 ppm for the ring carbons, the 90-Hz coupling of the latter carbon to its carbonyl resonating at 184 ppm, and the anomalous amide proton chemical shift of Ala32 (9.43 ppm) that follows modified Cys31. The latter signal (green arrow in D) clearly shows that only two Cys residues are modified.

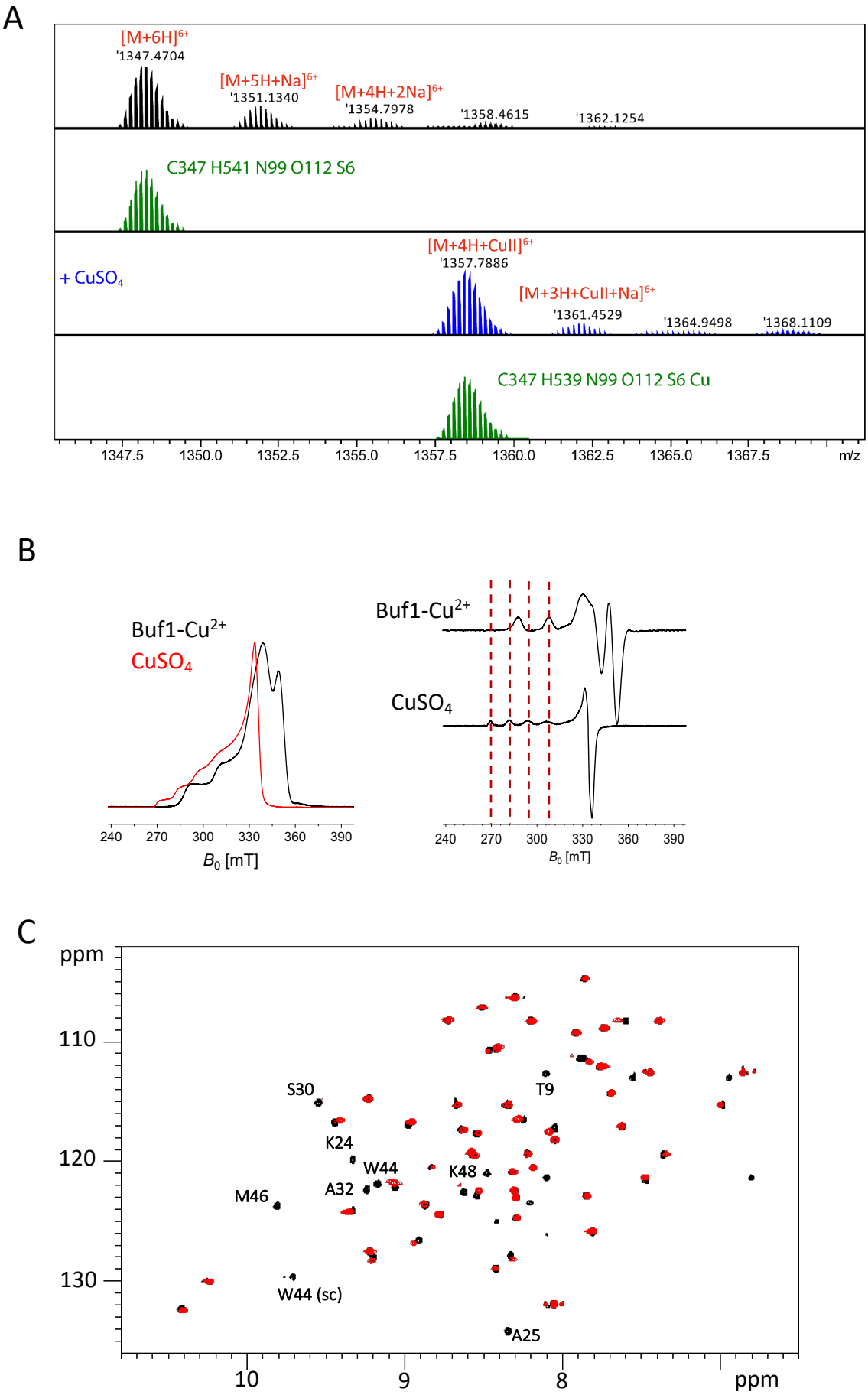

Fig. 4. Analyses of the Bufferin 1-copper complex formed *in vivo*. A. Native mass spectrometry analysis of Buf1^{str} purified from a copper-treated culture: enlargement of the isotopic patterns of the major charge state (6+). Upper two panels: purified Buf1^{str} from a non-supplemented culture; lower two panels: purified Buf1^{str} from *E. coli* cultures supplemented with $CuSO_4$. The calculated isotopic patterns for $[M+6H]^{6+}$ and $[M+4H+CuII]^{6+}$ species are shown in green. B. Evidence for Cu^{2+} binding to Buf1^{str} by EPR spectroscopy. Spectra of Echo-Detected Field-Swept (EDFS) of $CuSO_4$ (red line) and of the Bufferin 1-Cu^{2+} complex (black line) are shown. Differences with free $CuSO_4$ are generated by strongly coordinating ligands, i.e., in the first coordination sphere of Cu^{2+}. At the right, pseudo-modulation of the EDFS spectra. The bottom spectrum shows the four lines typical of free Cu^{2+} absent from the spectrum of the complex. C. Superposition of the ^{1}H, ^{15}N HSQC spectra of apo bufferin (black spots) and the *in-vivo* formed copper complex (red spots).

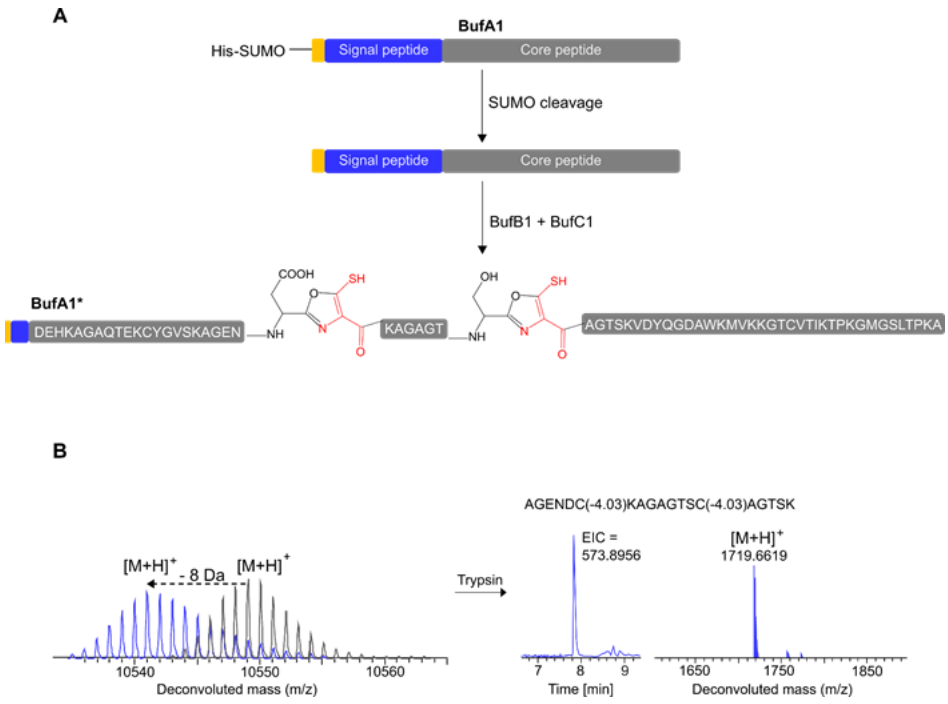

Figure 5. *In vitro* reconstitution of enzymatic activity. A. Workflow of *in vitro* assay. The purified His_6-SUMO-BufA1 was first subjected to proteolysis by SUMO protease, generating the precursor BufA1 with an additional 11 aa (IEENLYFQSNA) at the N-terminus. This peptide was subsequently used as a substrate for BufB1 and BufC1, yielding modified BufA1* with two thiooxazoles. The orange box represents the 11-residue sequence. B. MS analysis of the reaction product. *Left panel*: Deconvoluted mass ion of BufA1* ($[M+H]^+$ at *m/z* 10535.1631) after incubation with BufB1 and BufC1 (blue) compared to that of the control reaction ($[M+H]^+$ at *m/z* 10543.1846) (grey), showing a mass loss of 8 Da. The -10 Da and -12 Da forms are not seen here, notably because the reactions were performed in reducing conditions. *Right panel*: LCMS analysis of the 19-residue tryptic fragment from BufA1* generated in vitro. The extracted ion chromatogram (EIC) of $[M+3H]^{3+}$ (at *m/z* 573.8945) and the deconvoluted mass are shown.

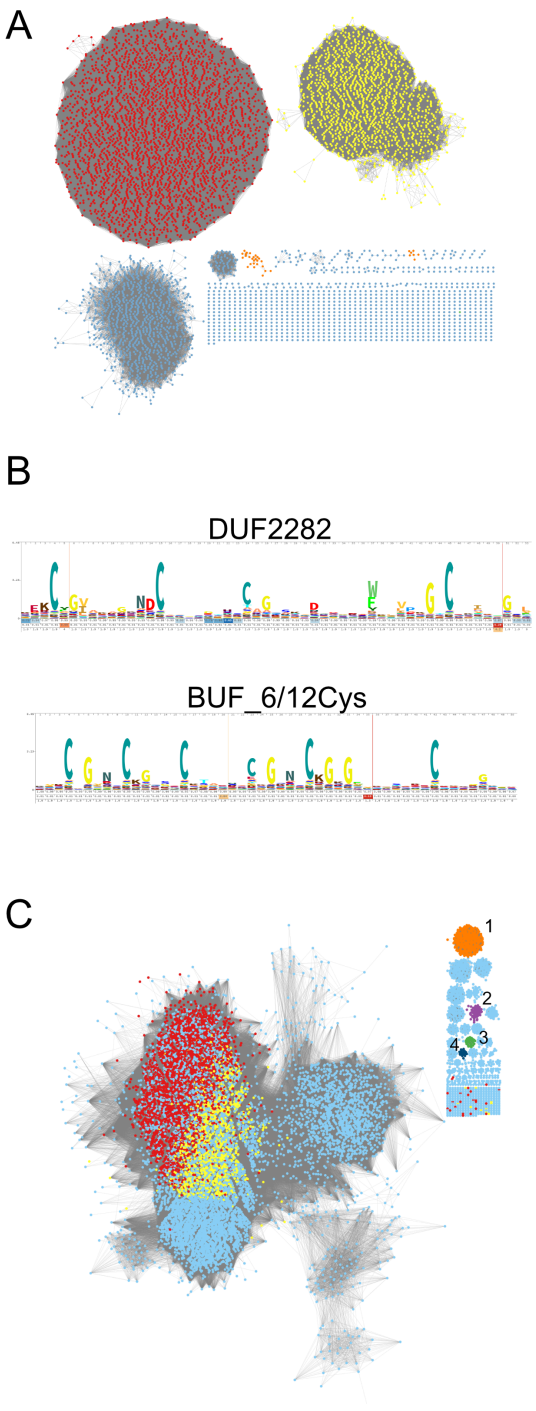

Figure 6. *In silico* analyses of the bufferin families. A. SSN analyses of the putative signal peptide-containing bufferin-like precursors genetically associated with MNIO enzymes. In the representative node network DUF2282 proteins, including BufA1 of *C. vibrioides*, belong to the largest cluster (red dots). The second largest cluster (yellow dots) represents proteins of the BUF_6/12Cys family that includes BufA2 of *C. vibrioides*. The previously described MNIO enzyme-modified RiPPs of *Chryseobacterium* are found in two small clusters (in orange). B. Weblogos for the major two families of bufferins. C. SSN analyses of MNIO enzymes. In the representative node network (at 80% identity), MNIO enzymes genetically associated with DUF2282 domain-containing proteins, including BufB1 of *C. vibrioides,* and with BUF_6/12Cys proteins, including BufB2 of *C. vibrioides*, are in red and yellow, respectively. MNIO enzymes that modify other known RiPPs - methanobactins, *Chryseobacterium* RiPPs, TglA-type pearlins and aminopyruvatides - are found in small, distinct clusters numbered 1 to 4 and shown in purple, orange, green and dark blue dots, respectively.

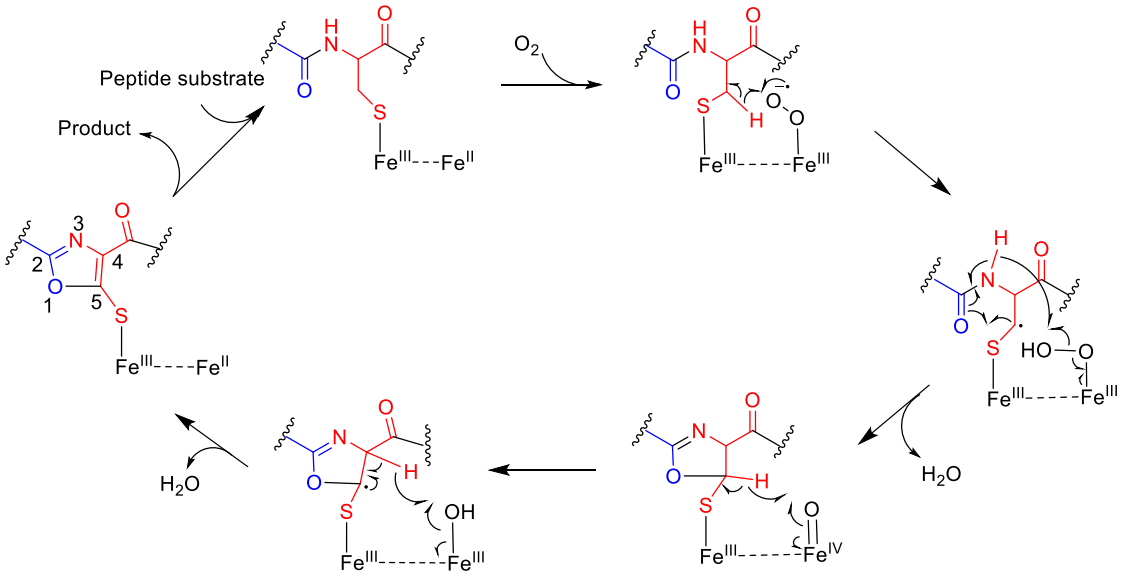

Figure 7. Possible mechanism of BufB2 to convert Cys into a 5-thiooxazole motif involving a mixed valent di-iron center. This process starts with O_2 activation and abstraction of a β-H followed by cyclization and ring oxidation.

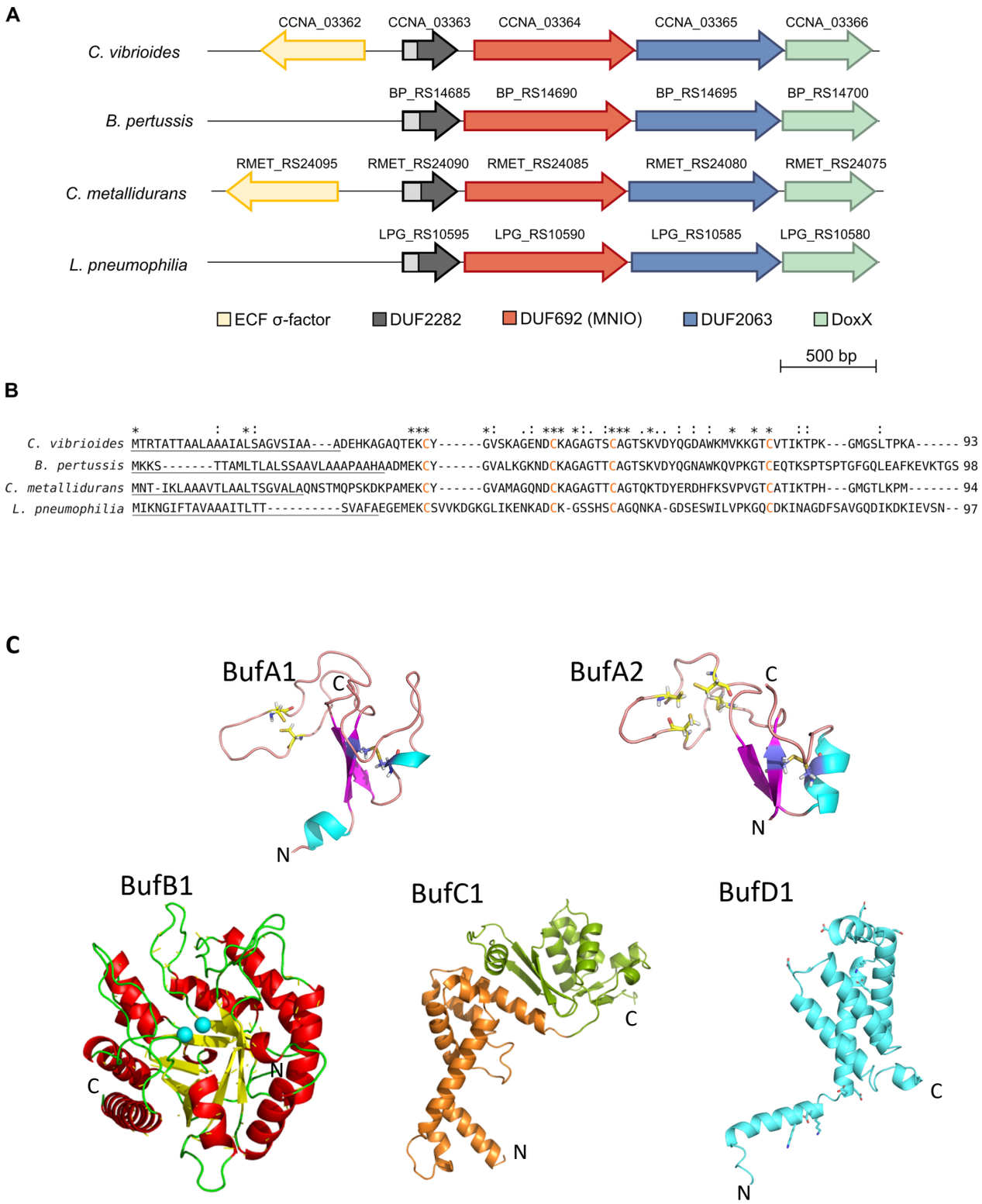

Extended Fig. 1. Main features of the *buf* BGCs. A. Gene organization of gold-induced genes (*gig*)-like operons found in the genomes of *C. vibrioides (C. crescentus)* (NC_011916.1), *B. pertussis* (NC_002929.2), *C. metallidurans* (NC_007974.2) and *L. pneumophilia* (NC_002942.5). Signal peptide-coding sequences are shown in pale grey in the DUF2282-coding genes. B. Sequence alignment of DUF2282-domain-containing proteins in *gig*-like operons. Predicted signal peptides are underlined and conserved cysteines are highlighted in orange. Consensus motifs are shown above the sequences. Sequence alignment was done by Clustal Omega. Signal peptides and cleavage sites were predicted using the SignalP 5.0 online tool. C. AlphaFold2 models for Buf1 and Buf2 (mature forms, after signal-peptide cleavage), BufB1, BufC1 and BufD1(DoxX) proteins of *C. vibrioides*. The BufC1 protein contains two domains, an all-α-helical DUF2063 domain (orange) and a RRE-like domain (green). In DoxX the 4-helix bundle is predicted to be inserted in the cytoplasmic membrane. N and C show the N and C termini of the proteins.

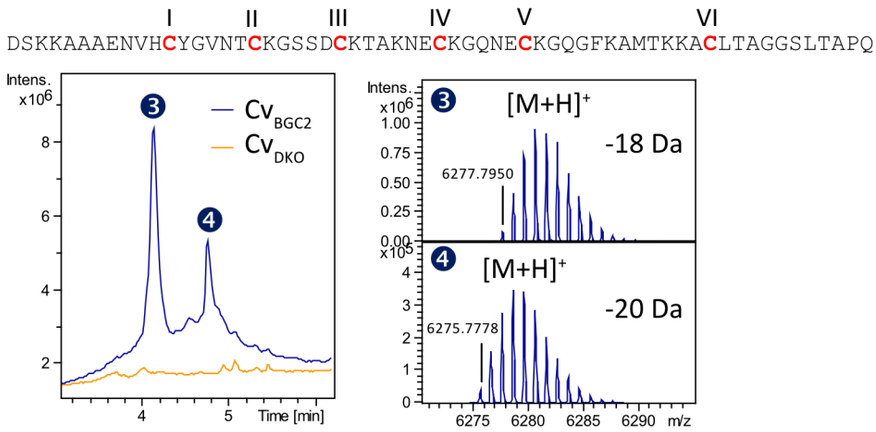

Extended Fig. 2. Top-down LC-MS analyses of bufferin 2. Top, sequence of Buf2 (core peptide) and bottom, LC-MS analyses of the cell extracts of Cv_{buf2}(pSigF) compared with Cv_{DKO}(pSigF). Left panel: total ion chromatogram, right panel: deconvoluted mass spectra of the two main peaks detected only for Cv_{buf2}. Two compounds were detected with masses corresponding to the expected core peptide (after removal of the signal peptide; calculated monoisotopic Mw 6294.96 Da), showing mass shifts of -18 Da ($[M+H]^+$ at *m/z* 6277.79) and -20 Da ($[M+H]^+$ at *m/z* 6275.78).

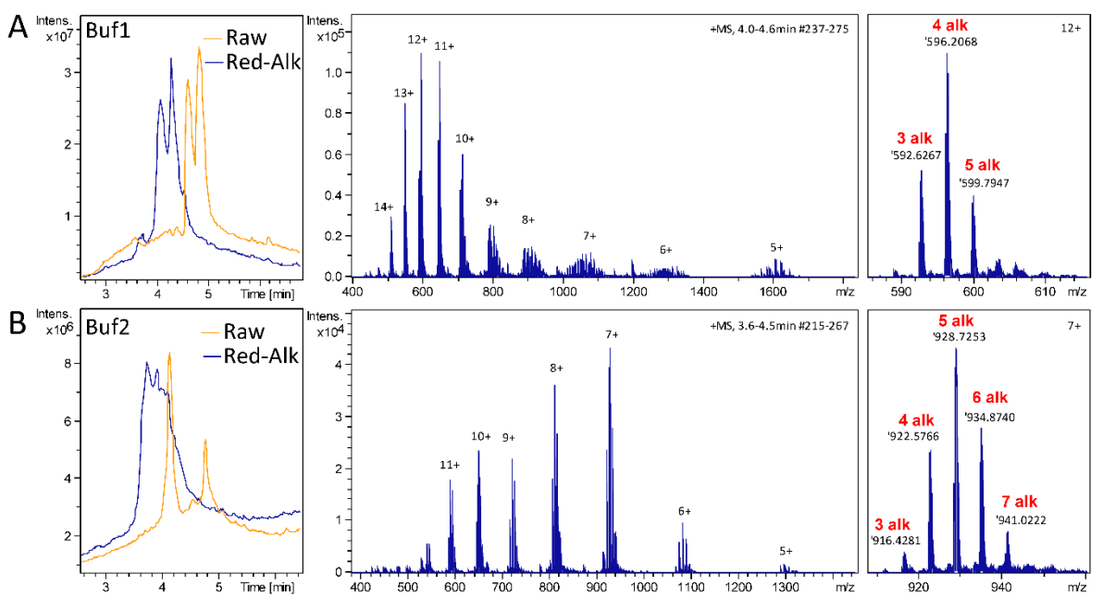

Extended Fig. 3. Reduction-alkylation of Buf1 and Buf2. Top-down LC-MS analyses of the cell extracts of Cv_{buf1}(pSigF) (A) or Cv_{buf2}(pSigF) (B) submitted to reduction and alkylation with 2-bromoethylamine. Total ion chromatograms compared to that of the untreated extracts (left panels), MS spectra of the main alkylated species detected (middle panels) and zooms on the major charge states (right panels). Minor species corresponding to additional unspecific alkylations (5 and 7 alkylations for Buf1 and Buf2, respectively) were also detected. These data indicate that the presumed PTMs of the Cys residues result in alkylation-sensitive groups.

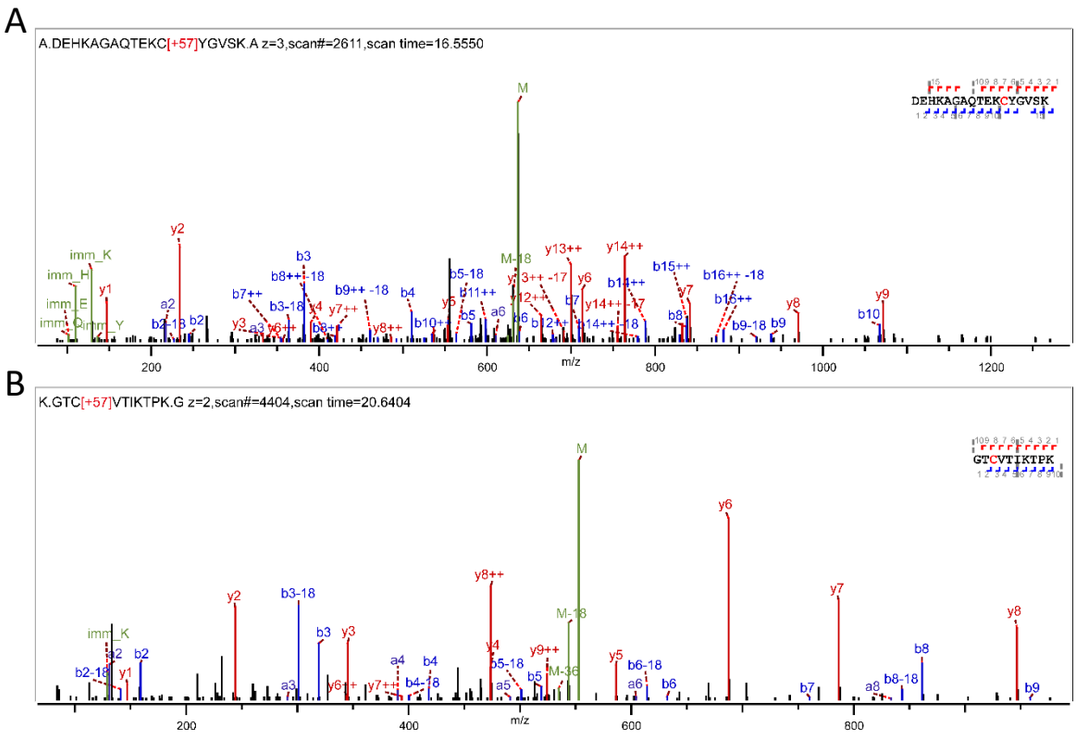

Extended Fig. 4. Bottom-up analysis of Bufferin 1. MS/MS spectra of the tryptic peptides containing the Cys^{I} and Cys^{IV} residues, DEHKAGAQTEKCYGVSK ($[M+3H]^{3+}$ at *m/z* 636.63)(A) and GTCVTIKTPK ($[M+2H]^{2+}$ at *m/z* 552.81) (B). The two Cys residues carry each a carbamidomethyl group resulting from alkylation with iodoacetamide (+ 57.02 Da).

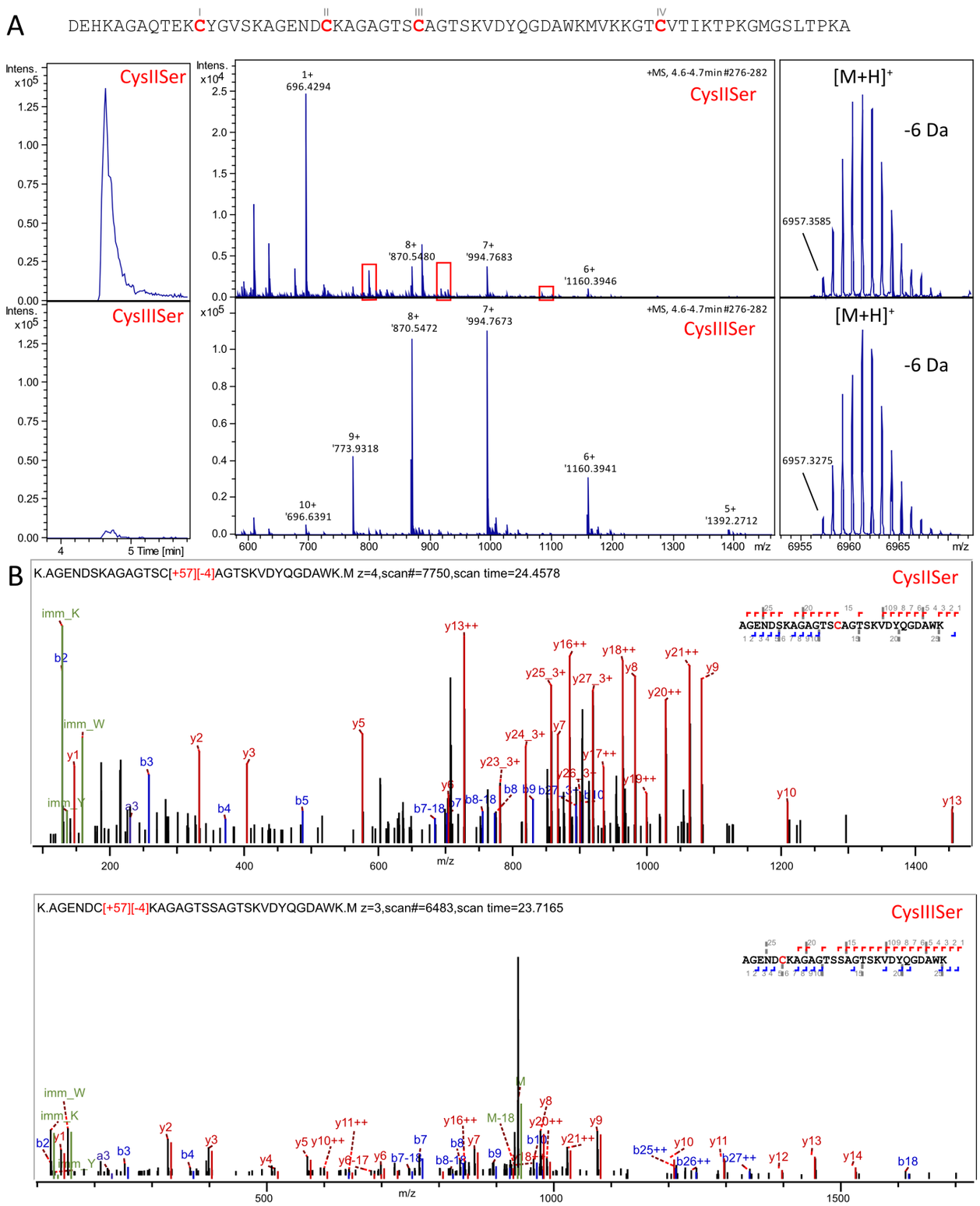

Extended Fig. 5 Analysis of the Cys^{II}Ser and Cys^{III}Ser variants of Buf1. A. Sequence of Buf1 and top-down LC-MS analyses of the cell extracts of $Cv_{buf1}{}^{CysIISer}$(pSigF) or $Cv_{buf1}{}^{CysIIISer}$(pSigF). Extracted ion chromatograms of the $[M+7H]^{7+}$ species of Buf1^{CysIISer} or Buf1^{CysIIISer} (*m/z* 995) (left), corresponding mass spectra (middle) and deconvoluted spectra (right). The measured *m/z* values (deconvoluted $[M+H]^{+}$ species at *m/z* 6957.36 and 6957.33 for Buf1^{CysIISer} and Buf1^{CysIIISer}, respectively) show -6 Da mass shifts from the masses expected for the proteins with no PTM (calculated monoisotopic Mw 6962.376951). This most likely corresponds to an S-S bond between Cys^{I} and Cys^{IV} and a - 4 Da mass shift for the remaining Cys residue (Cys^{II} or Cys^{III}). B. MS/MS spectra of the tryptic peptides AGEND**S**KAGAGTS**C**AGTSKVDYQGDAWK for Buf1^{CysIISer} ($[M+4H]^{4+}$ at *m/z* 707.56) and AGEND**C**KAGAGTS**S**AGTSKVDYQGDAWK for Buf1^{CysIIISer} ($[M+3H]^{3+}$ at *m/z* 943.08). For both variants, the unsubstituted Cys carry a carbamidomethyl group resulting from alkylation with iodoacetamide (+ 57.02 Da), together with a -4.03 Da mass shift.

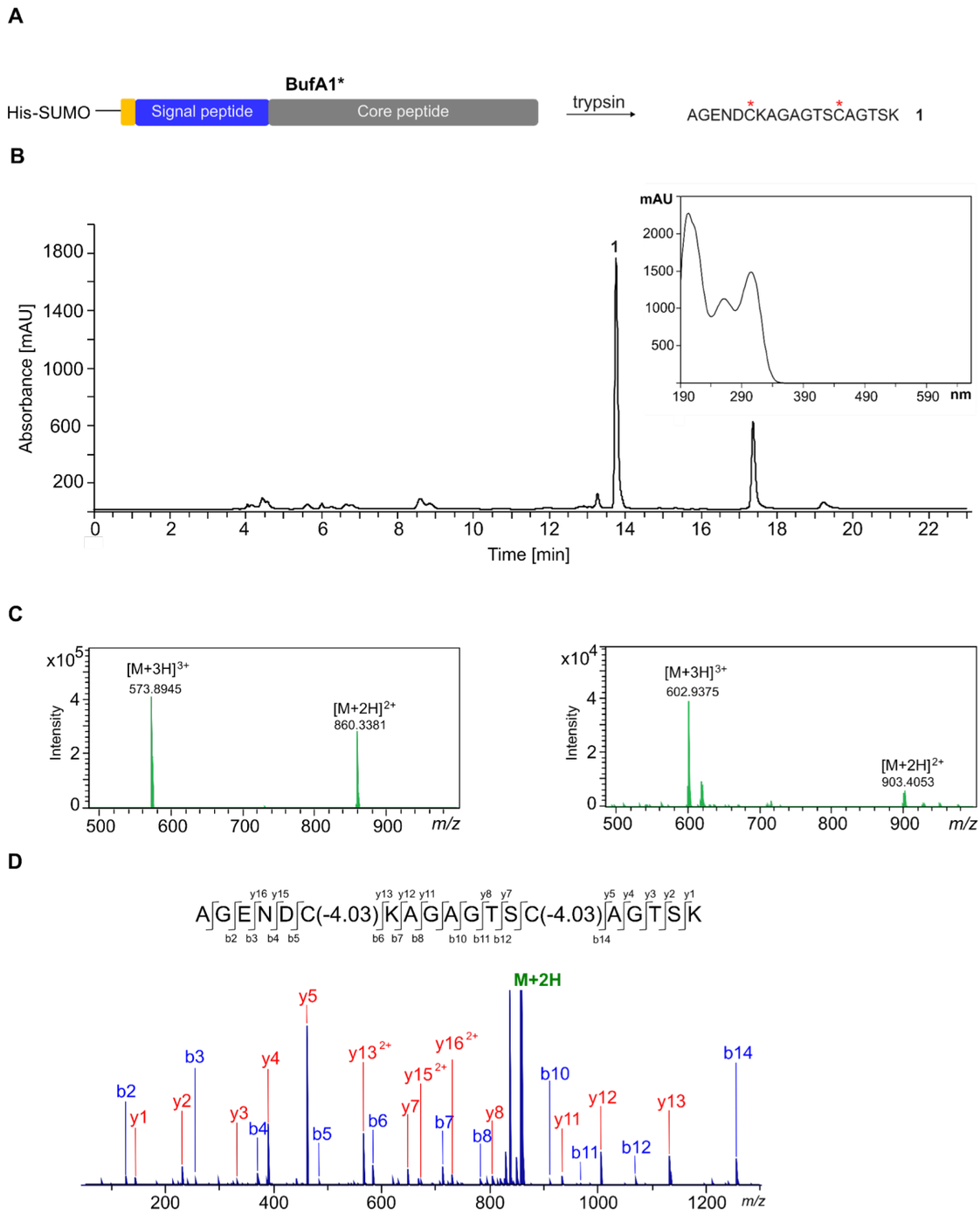

Extended Fig. 6. *In vivo* production and purification of the central tryptic peptide. A. Modified BufA1* was produced through co-expression with BufB1 and BufC1 in *E. coli* and purified via Ni-affinity chromatography. The obtained peptide was digested with trypsin generating the 19-residue peptide 1 containing modifications on the two Cys residues (marked with *). B. Chromatogram of HPLC purification (UV = 280 nm). The peak at RT = 13.85 min was collected and corresponds to peptide 1. The inset shows the corresponding UV/vis scan exhibiting a new absorbance maximum at 305 nm. C. Mass spectrum of purified unlabelled (left panel) and ^{13}C- and ^{15}N-labelled peptide 1 (right panel). D. MS/MS spectrum of the central tryptic peptide ($[M+H]^{3+}$ at m/z 573.8945).

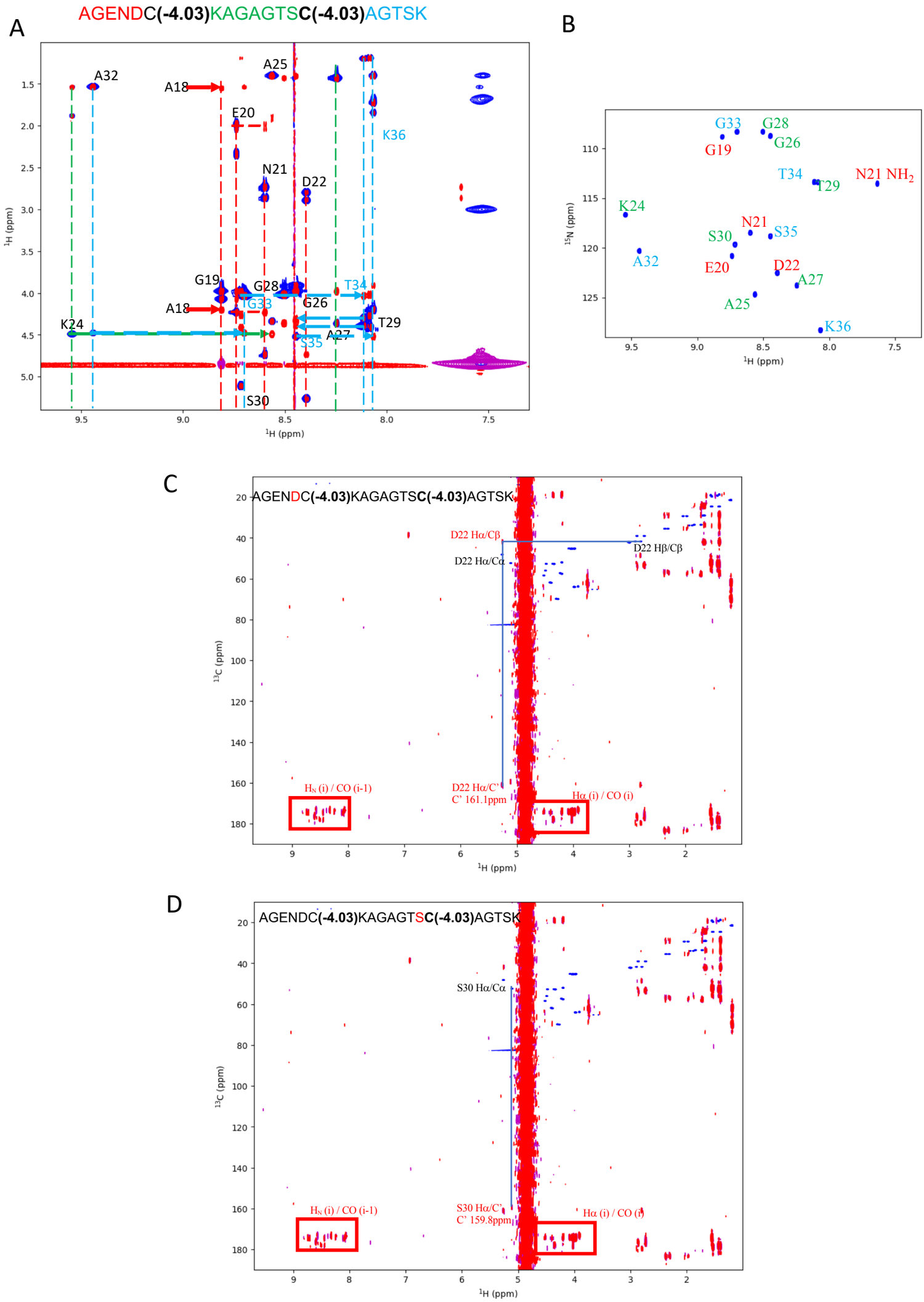

Extended Fig. 7 NMR experiments to assign the resonances of the 19-mer peptide (A18-K37). A. ROESY/Tocsy experiments. B. Natural abundance ^{1}H, ^{15}N HSQC spectrum. C and D. ^{1}H, ^{13}C HMBC experiments on the 19-mer peptide at natural isotopic abundance.

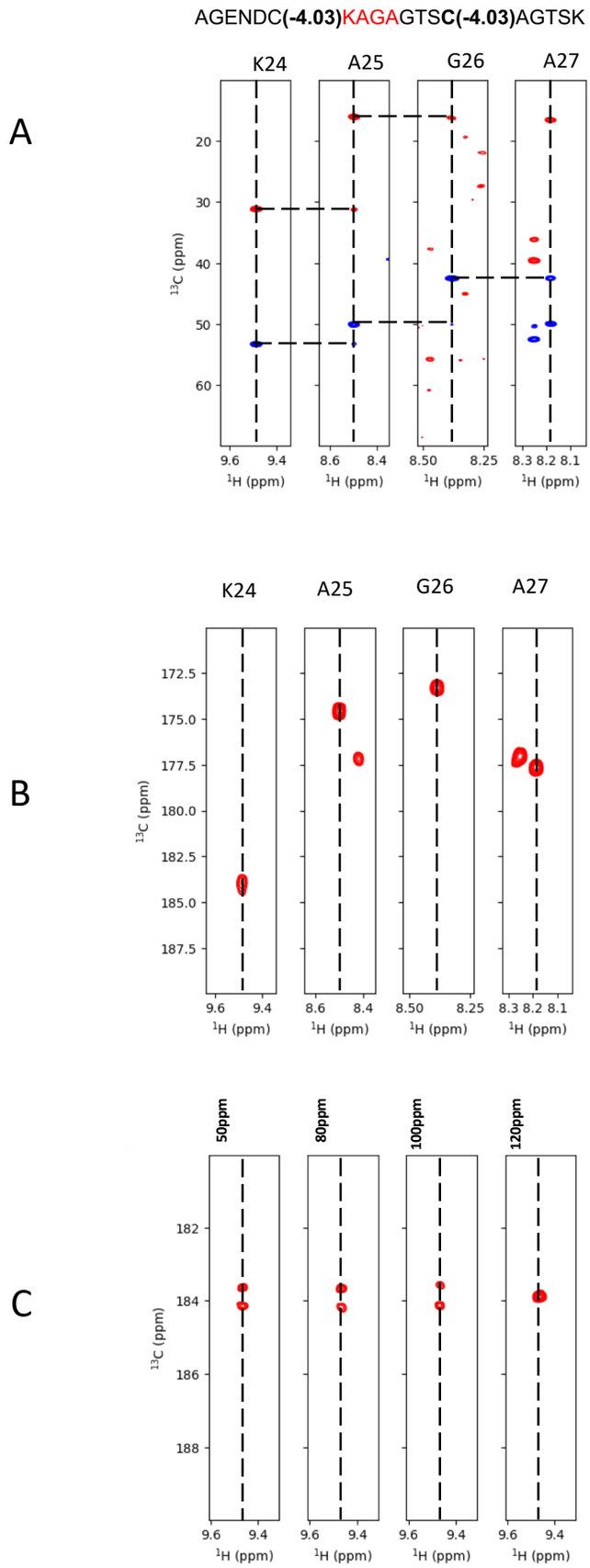

Extended Fig. 8. NMR experiments on the uniformly ^{13}C, ^{15}N labelled 19-mer peptide. A. HNCACB experiment. Sequential walk shown here for the sequence following Cys^{II} (Lys24-Ala27). For Lys24 we did not find any resonances that could correspond to its upstream neighbour, whereas for downstream residues the amide resonance of a given residue X*i* is coupled both to its own Cα/Cβ and the Cα/Cβ resonances of the preceding (X*i*-1) residue. B. The HNOC plane shown at the ^{15}N frequency of the indicated residues. Whereas we find classical values around 175 ppm for all residues of the peptide, the residues downstream of a modified Cys resonate at 184 ppm (B). C. HNOC spectrum. Shown is the HNCO plane through the resonance of Ala32 (that immediately follows Cys^{III}) while modifying the offset of the decoupling pulse during the C=O evolution period.

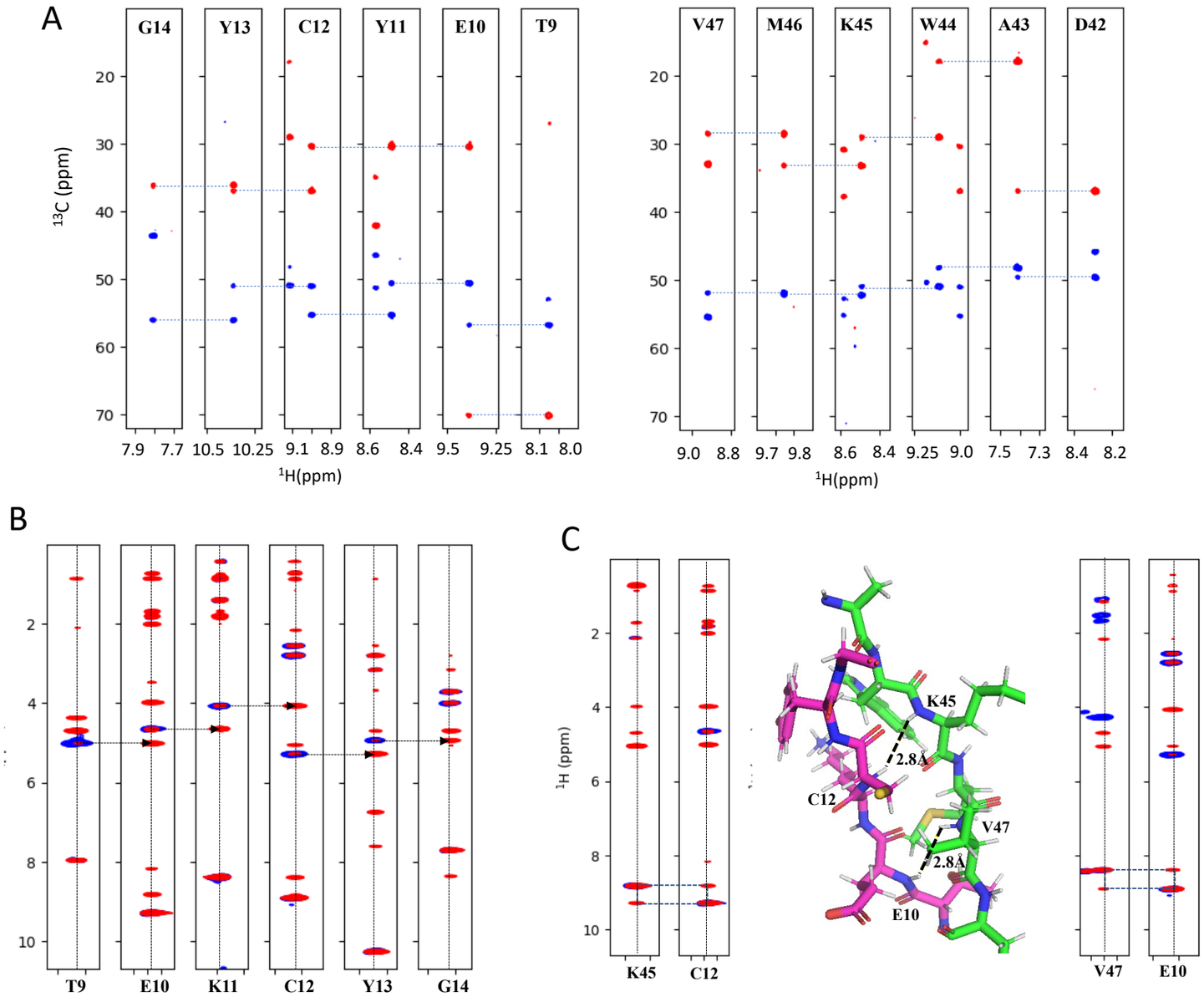

Extended Fig. 9. Structural characterization of bufferin 1. A. HSQC-NOESY and TOCSY experiments: sequential walks through residues of the first and second β strands, respectively. B. Strips from TOCSY-HSQC (blue) and NOESY-HSQC (red) spectra of bufferin 1. Characteristic Hα(i-1) – HN(i) NOE contacts are indicated by arrows. These data confirm the assignement and demonstrate the extended (β strand) nature of this segment. C. Strips through the TOCSY-HSQC (blue) and NOESY-HSQC (red) spectra of bufferin 1. These data show the inter-strand HN-HN NOE contacts, confirming the presence of an anti-parallel β sheet.

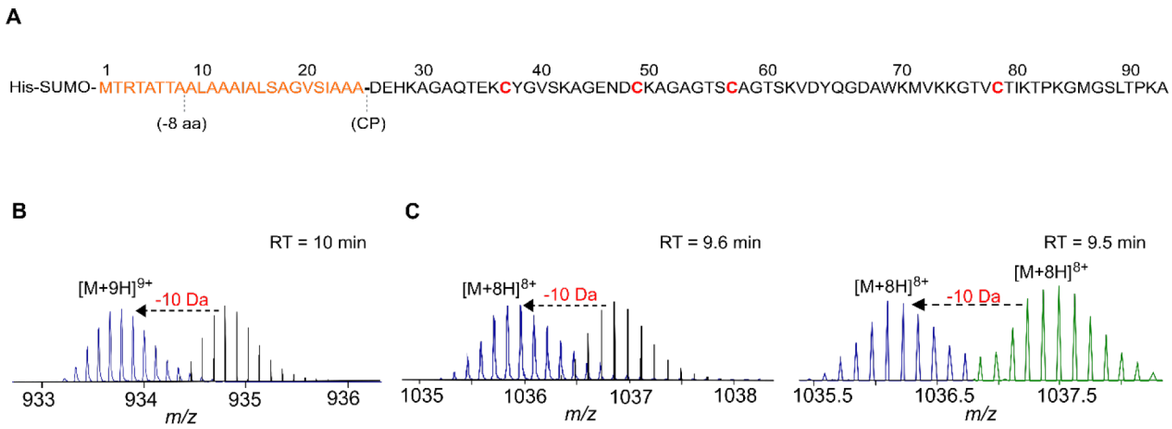

Extended Fig. 10. The signal-peptide sequence is not essential for heterocycle formation. A. Schematic illustration of variant BufA1 with signal peptide truncations. The signal peptide is in orange, and the four Cys in the core peptide are highlighted in red. B. LCMS analysis of modified BufA1(-8aa). MS spectrum of the most abundant charge state $[M+9H]^{9+}$, corresponding to a deconvoluted monoisotopic mass $[M+H]^{+}$ of 8391.1281, is shown (blue) and compared to the theoretical spectrum of unmodified peptide (black). C. LCMS analysis of modified BufA1(CP). *Left panel*: The fully converted peptide was eluted at RT 9.6 min. The MS spectrum of the most abundant charge state $[M+8H]^{8+}$, corresponding to a deconvoluted monoisotopic mass $[M+H]^{+}$ of 8277.9398, is shown (blue) and compared to the theoretical spectrum of unmodified peptide (black). *Right panel*: unmodified peptide (green) was eluted with the modified one (blue) at RT 9.5 min. Its MS spectrum of the charge state $[M+8H]^{8+}$, corresponding to a deconvoluted monoisotopic mass $[M+H]^{+}$ of 8287.8888, is shown.